Pergamon

Geochimica et Cosmochimica Acta, Vol. 58, No. 12, pp. 2689–2710, 1994

0016-7037/94 $6.00 + .00

0016-7037(94)00067-0

Roter Kamm impact crater, Namibia: Geochemistry of basement rocks and breccias

WOLF UWE REIMOLD,[1] CHRISTIAN KOEBERL,[1,2,*] and JANICE BISHOP[2,3]

[1]Economic Geology Research Unit at the Department of Geology, University of the Witwatersrand, Johannesburg 2050, South Africa
[2]Institute of Geochemistry, University of Vienna, Dr.-Karl-Lueger-Ring 1, A-1010 Vienna, Austria
[3]Department of Chemistry, Brown University, Providence, RI 02912, USA

(*Received September* 9, 1993; *accepted in revised form February* 7, 1994)

Abstract—The Roter Kamm crater in the southern Namib Desert has previously been identified as an impact structure on the basis of crater morphology and the presence of impact melt breccias which contain shock metamorphosed quartz and lithic clasts. To better define the variety of target rocks and breccias, we studied the petrography and chemical composition of a new suite of twenty-eight basement and breccia samples from the Roter Kamm crater. Based on chemical data for target lithologies and breccias we suggest that the crater was formed in a two-layer target region: an upper layer of Gariep metasediments (schist, marble, ± quartzite and sandstone) overlying the crystalline basement of the Namaqualand Metamorphic Complex. The basement was also heavily intruded by coarse-grained quartz veins and quartz- and quartz-feldspar pegmatites. The clast population in the melt breccias indicates that impact-induced melting involved mainly metasedimentary target rocks, with rarely detected contributions from pegmatite and granite/granodiorite. Three varieties of melt breccias can be defined: (1) "schistose," (2) quartzitic melt breccias, and (3) "true" impact melt breccias. These melt breccia types are chemically heterogeneous, and even the impact melt breccias may have been produced in situ and not from a coherent melt body. The shapes of the schistose melt breccias, previously thought to be ejected impact breccias, are most likely caused by erosion, and these breccias are now interpreted to be locally derived.

The crater basement as exposed at the rim was structurally severely affected and, at least locally, considerable thermal energy was generated during formation of large volumes of cataclastic, mylonitic, and pseudotachylitic breccias. Analyses of mylonite and pseudotachylites from the crater rim, as well as their respective host rocks, show that these breccias were mainly formed from local material. Analyses of pseudotachylite-like breccias indicate that these possible friction melts are generated by preferential melting of hydrous ferromagnesian minerals and feldspar, similar to their tectonically produced counterparts. Although no significant fluid effects resulting from formation of mylonites or pseudotachylites are indicated, several breccias (compared to their host rocks) do show evidence of severe chemical alteration (chloritisation and sericitisation). The presence of large vesicles filled with hydrothermal mineral assemblages in some schistose breccias and other petrographic and chemical data support the hypothesis of an impact-induced hydrothermal event in the crater area.

INTRODUCTION

THE 2.5 km DIAMETER, near-circular Roter Kamm crater in southern Namibia is located at 27°46′S and 16°18′E in the Namib Desert, about 80 km due north of Oranjemund. It is situated within the restricted "Sperrgebiet" and is not easily accessible. Figure 1a,b shows the crater from space and from the air, respectively. Based on preliminary morphological and field observations, an impact origin for this crater structure was proposed by DIETZ (1965) and later FUDALI (1973). The impact origin was confirmed in the late 1980s by a detailed geological study of the crater and the discovery of clasts in impact melt breccias with characteristic shock deformation features indicative of shock pressures up to 30 GPa (e.g., MILLER and REIMOLD, 1986; REIMOLD and MILLER, 1987). Rock deformation in basement rocks exposed along the crater rim includes locally dense jointing and cataclastic, mylonitic, and pseudotachylitic breccias occurring in the form of individual veins or in up to 60 m wide radial breccia zones, as well as in rim-parallel veins (Figs. 2, 3). Breccias, similar in shape to the so-called "flädle" from the Nördlinger Ries crater, were found exclusively at the northern rim of the crater. A few of these breccias contain basement rock clasts displaying shock effects, such as planar deformation features in quartz or diaplectic quartz glass (REIMOLD and MILLER, 1989). Breccias from this part of the rim consist of mica schist with intercalated quartzitic bands and occasional pockets or schlieren of recrystallized melt, sometimes containing small clasts of other basement lithologies. They were accordingly termed "schistose" melt breccias (REIMOLD and MILLER, 1989; KOEBERL et al., 1990a). The amount of deformation present in the crater rim is unusual for a small impact crater.

Basement rocks of the crater area consist of granitic and granodioritic orthogneisses of the 1200–900 Ma old Namaqualand Metamorphic Complex (NMC), which are thoroughly invaded by quartz-feldspar pegmatite intrusions and coarse-grained quartz veins. A thin discontinuous veneer of late Proterozoic Gariep (ca. 700 Ma) metasediments, namely calcareous sandstones, marble with minor chert, and schist covered the Namaqualand gneisses. The crater rim is almost totally covered by dune sand and the interior is filled with

* Author to whom correspondence should be addressed (Vienna).

FIG. 1. (a) The Roter Kamm crater and, on the right side, the Aurusberg mountains in the southern Namib desert; northeast is to the right (Space Shuttle photograph 61C-40-001). (b) Oblique aerial view of the Roter Kamm crater, looking south.

partially vegetated aeolian sand deposits (Figs. 1b, 2). The age of the Roter Kamm crater was the subject of various studies (STORZER et al., 1990; HARTUNG et al., 1991) and has recently been shown to be 3.7±0.3 Ma (KOEBERL et al., 1993). This age is close to the lower limit of earlier estimates of 5 to 30 Ma (REIMOLD and MILLER, 1989) based on findings of calcrete with melt breccia inclusions just outside the crater (discussed in more detail in the present paper).

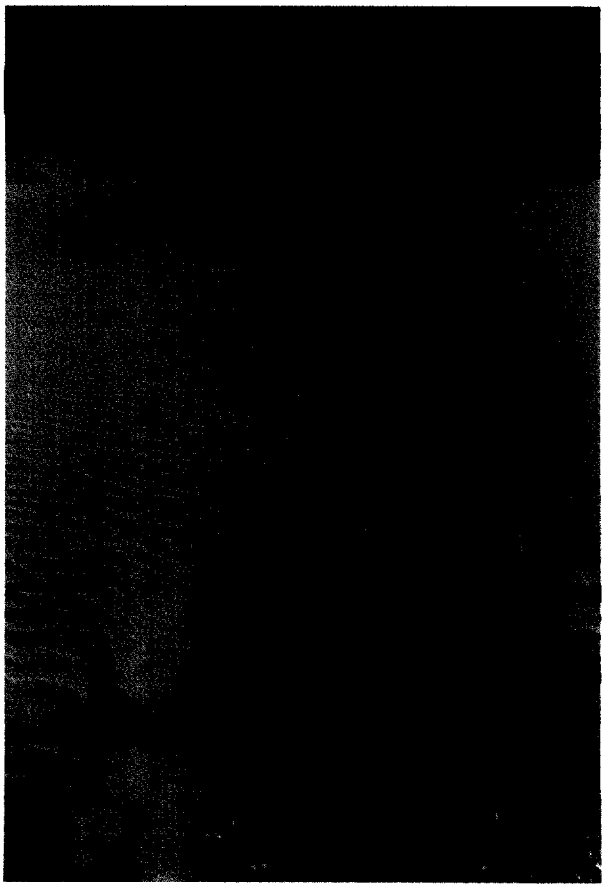

FIG. 2. Massive pseudotachylite partially exposed on the slope of the high dune on the southeastern crater rim. Field of view about 6 m at the base of photograph.

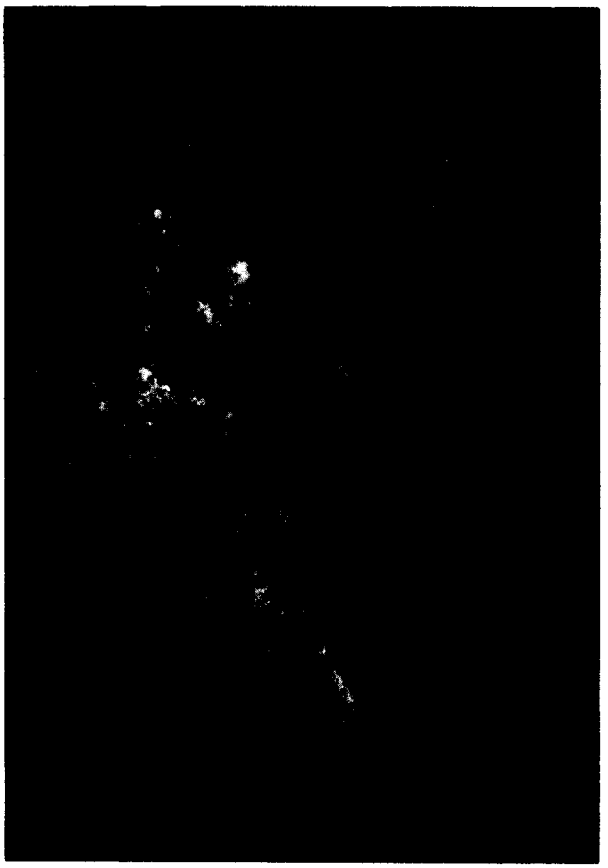

FIG. 3. Network of millimeter and submillimeter wide veinlets of pseudotachylite-like breccia between two several millimeter thick possible generation planes, in granodiorite sample 37 collected in situ on the southern rim.

REIMOLD and MILLER (1989) studied the petrological and chemical characteristics of a variety of Roter Kamm basement rocks and breccias. They showed that the basement lithologies consist mainly of relatively fresh, undeformed, and weakly to well-foliated orthogneisses. Three types of (undeformed) xenoliths were observed in the gneissic basement: amphibolites, aplites, and a small body of quartz-hornblende granulite. In addition, massive bodies and large veins of possibly pegmatite-derived quartz and quartz plus feldspar are ubiquitous along the rim crest (REIMOLD and MILLER, 1989). Due to the very limited outcrop, it is not clear if the quartz and quartz-feldspar bodies and veins are indeed associated with pegmatite intrusions. The coarse nature of these rocks makes it very difficult to obtain a representative sample for chemical analysis.

Pseudotachylitic and cataclastic or mylonitic breccias were reported from the Roter Kamm crater (REIMOLD and MILLER, 1989). However, no consensus has yet been reached about the existence of true pseudotachylites at Roter Kamm, nor about the nomenclature used to describe such rocks. The terminology used in the literature is confusing and not consistent (see, e.g., REIMOLD et al., 1987; REIMOLD and MILLER, 1989; REIMOLD, 1991; MAGLOUGHLIN and SPRAY, 1992). In general, pseudotachylites are described as containing evidence of melting and clasts therein are devoid of shock metamorphic features. REIMOLD and MILLER (1989) found some samples which they classified as pseudotachylites because they contain devitrified glass and other evidence of melting (their Fig. 7c) but lacked evidence for shock metamorphism (e.g., their Fig. 11b). On the other hand, DEGENHARDT et al. (1992, 1994) have studied similar fine-grained, clast-rich veins and dikes and failed to find evidence for melting. However, even though such breccias should then be called cataclasites, DEGENHARDT et al. (1994) prefer to call them pseudotachylites anyway, thus adding to the confusion. Regarding the occurrences at Roter Kamm, the scarcity of outcrop makes it difficult to distinguish between "classic" pseudotachylites and impact breccias that show evidence of melting but were formed in situ due to shock compression, not by fault-related frictional melting. A further problem is that in small craters evidence for shock metamorphism in crater rim or floor rocks is generally limited, thus making it difficult to identify "true" impact breccias.

Chemical and petrographic data are presented for twenty-eight Roter Kamm samples, in addition to those discussed by REIMOLD and MILLER (1989). This suite includes a larger variety of country rocks, in situ mylonitic and pseudotachylitic breccias, as well as schistose and quartzitic melt-bearing

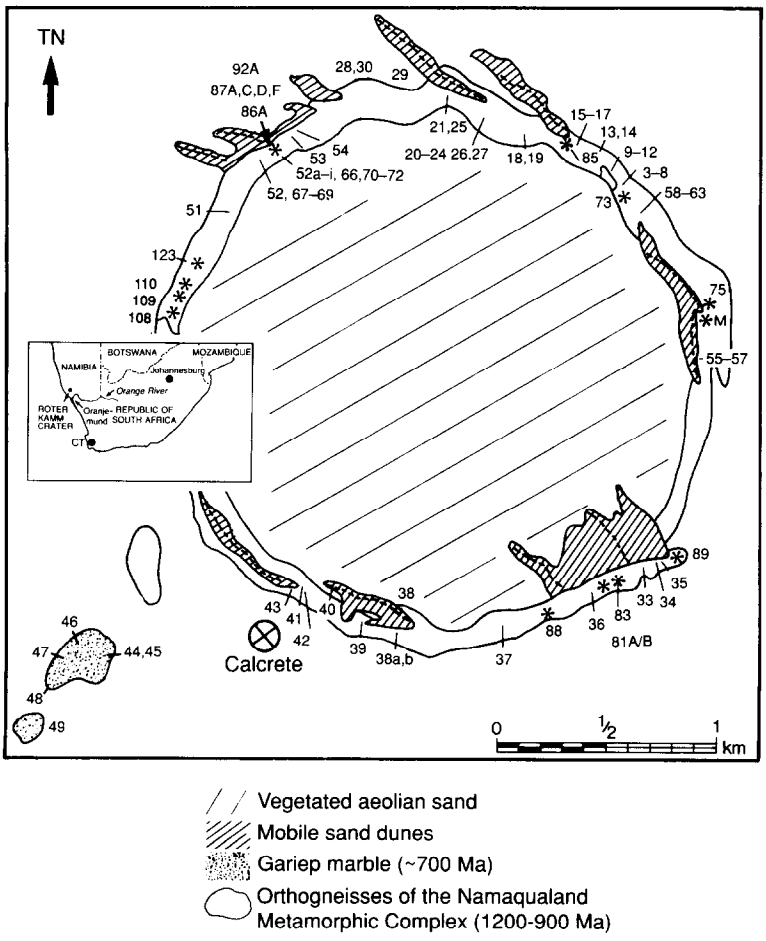

FIG. 4. Sampling localities in the Roter Kamm crater for all samples discussed by REIMOLD and MILLER (1989) and in this study (marked with * on the map). Inset: Locality of the crater structure in the southern Namib desert of Namibia (CT = Cape Town).

breccias. Previously, schist and pegmatite were recognized as principal components of the then so-called ejecta breccias (REIMOLD and MILLER, 1989). Here, we try to define better the variety of target rocks present (including pegmatites and schist) in the crater area, as well as enlarge the database for various types of melt breccias. In addition, four pseudotachylite and mylonite samples were analyzed together with their respective host rocks to investigate any chemical changes that might have occurred during the formation of such breccias. Furthermore, we present additional evidence for a post-impact hydrothermal event, as proposed by KOEBERL et al. (1989, 1990b). The data presented in this work are integrated with data for samples given by REIMOLD and MILLER (1989). To distinguish between new data and samples discussed by REIMOLD and MILLER (1989), sample numbers from the previous paper are designated in the text with an asterisk (*).

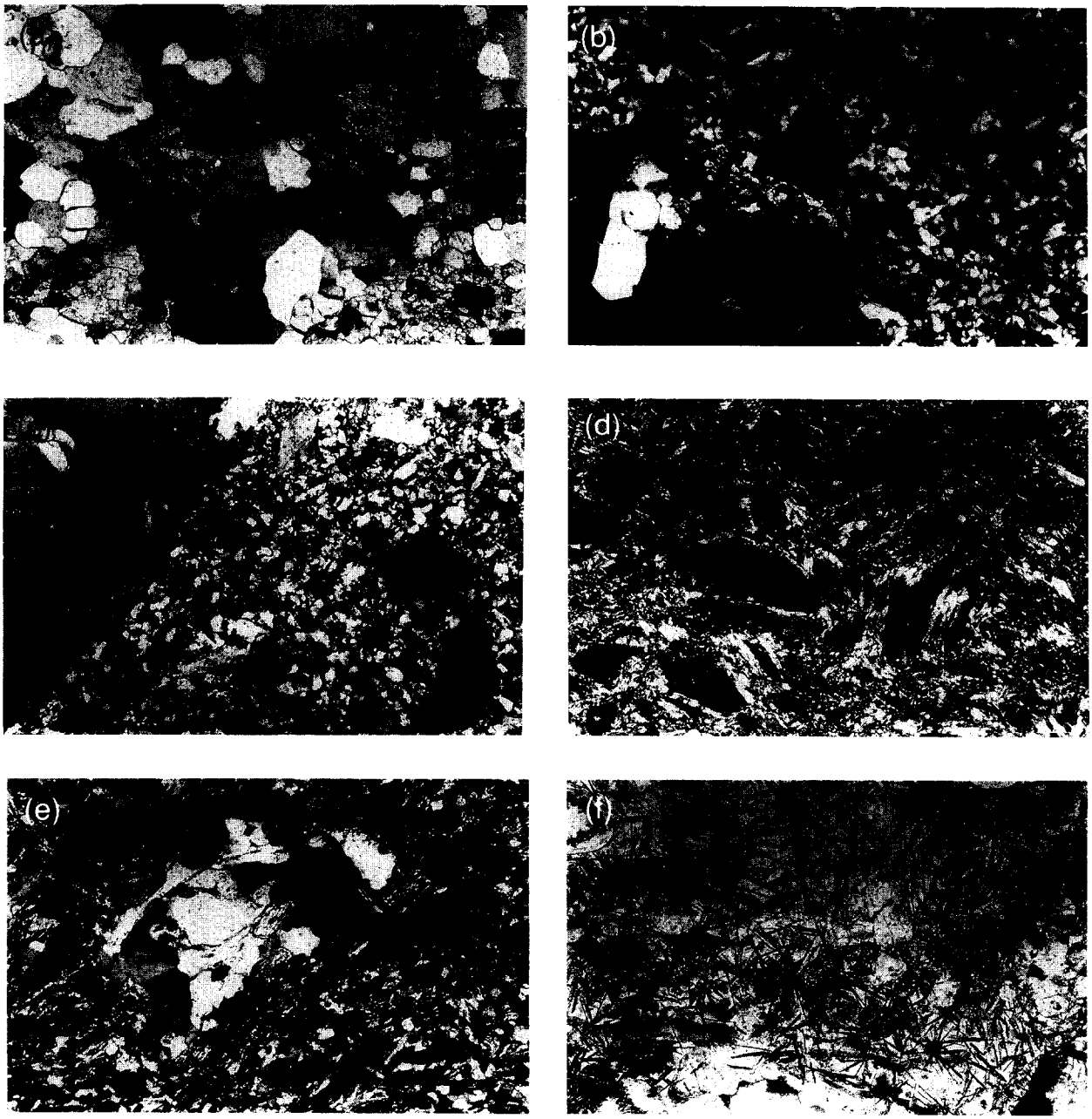

FIG. 5. Photomicrographs of selected samples: (a) calcareous sandstone URK-73A (crossed nicols, width: 2.2 mm); (b) quartzitic melt breccia URK-87A with quartz-microcline clast (crossed nicols, width: 1.75 mm); (c) monomict breccia URK-81A, mylonitic band (crossed nicols, width 1.4 mm); (d) schistose melt breccia URK-52H (analyzed by REIMOLD and MILLER, 1989) with oxidized siltstone clast set in partially fused and annealed matrix (light grains are quartz or, when lath-shaped, muscovite; crossed nicols, width 2.2 mm); (e) partially fused (bottom right) shale URK-77 with quartzitic clast (crossed nicols, width: 2.2 mm); (f) melt breccia URK-41: glassy matrix with pyroxene crystallites (parallel nicols, width: 2.2 mm; compare also to Fig. 9e, f of REIMOLD and MILLER, 1989).

TABLE 1. MAJOR AND TRACE ELEMENT COMPOSITION OF TARGET ROCKS FROM THE ROTER KAMM IMPACT CRATER.

	NAMAQUALAND METAMORPHIC COMPLEX													GARIEP
	PEGMATITES		ORTHOGNEISSES						APLITES		LOCALLY BRECCIATED PEGMATITE	ORTHOGNEISSES		CALC. SANDST.
	123	75	85	88	89	108	109	110	21	38B	83	81A	81B	73A
SiO_2	98.19	85.47	76.34	74.89	72.50	55.91	59.62	47.78	76.02	82.51	92.79	60.19	66.81	64.73
TiO_2	0.01	0.25	0.03	0.10	0.24	0.64	0.65	0.85	0.06	0.10	0.02	0.44	0.26	0.02
Al_2O_3	0.71	5.02	13.61	12.84	13.72	20.90	16.14	12.30	12.32	6.97	3.17	16.46	14.07	0.21
Fe_2O_3	0.40	3.95	0.45	0.99	2.34	4.56	7.16	12.01	0.87	2.83	0.56	5.23	3.74	0.26
MnO	0.02	0.06	0.01	0.01	0.05	0.09	0.12	0.40	0.02	0.02	0.01	0.12	0.08	0.02
MgO	0.01	1.49	0.04	0.41	0.78	3.12	3.36	11.64	0.38	0.49	0.01	2.19	1.35	7.70
CaO	0.03	0.51	0.58	0.95	1.39	2.23	5.95	7.24	0.44	3.86	0.10	1.74	0.81	10.87
Na_2O	0.77	0.89	6.32	4.09	4.51	6.28	2.64	0.79	3.90	1.08	0.12	1.71	0.74	0.08
K_2O	0.21	1.83	2.11	4.48	3.99	3.65	2.50	3.44	6.15	0.77	2.26	10.28	10.21	0.02
P_2O_5	0.01	0.04	0.02	0.03	0.08	0.36	0.20	0.24	0.03	0.07	0.02	0.23	0.10	0.03
L.O.I.	0.18	0.15	0.60	0.59	0.69	1.49	1.49	2.90	0.50	0.89	0.26	1.74	1.20	15.71
Total	100.54	99.66	100.11	99.38	100.29	99.23	99.83	99.59	100.69	99.59	99.32	100.33	99.37	99.65
Sc	0.33	0.34	1.5	2.16	4.92	21.5	17.5	22.5	0.82	2.92	0.60	9.6	6.8	0.16
V	23	9.2	19	20	29	126	173	194	18	64	21	104	92	13.4
Cr	133	51	49	126	133	39.9	22.8	230	297	262	142	79	89	76
Co	0.35	0.74	1.1	1.82	4.08	13.2	24.4	65.1	1.43	2.38	1.9	19	15	0.37
Ni	<1.4	4.4	6	11	19	21	15	170	<10	22	3	26	28	<2
Cu	<2	<2	15	1.8	22.5	<1	<1	<1	9.8	5.8	<2	157	204	<2
Zn	1	3	11	12.1	39.6	101	109	255	7.6	9.2	2	40	30	2
Ga	<3	14	<8	8.3	11	8	10	5	4.8	7.5	5.2	13	16	<1
As	<0.2	<0.2	0.1	0.30	0.32	1.62	1.55	1.32	0.3	0.31	0.2	0.2	0.3	0.2
Se	0.5	<0.05	<0.1	2.1	3	0.8	0.3	0.4	1.3	0.9	<0.1	<0.1	<0.1	<0.1
Br	0.8	<1	1.2	0.28	0.3	0.31	0.25	0.66	<1.5	<1	<1	1.5	1.4	<1
Rb	10	300	70	152	170	147	110	298	234	36	90	670	740	<0.7
Sr	1	158	54	135	150	199	515	92	169	330	42	281	172	18
Y	3.0	10.1	53.0	14.0	17.9	18.9	14.6	21.2	9.0	6.8	5.9	34	37	3.5
Zr	13	21	126	95	71	204	98	79	76	98	19	199	124	26
Nb	<0.5	1.4	7.8	9.7	8.9	12.5	5.8	7.6	1.8	1.8	0.7	10	8.5	1.7
Sb	0.12	0.11	0.06	0.15	0.26	0.077	0.096	0.26	0.19	0.06	0.08	0.37	0.32	0.01
Cs	0.45	1.1	0.59	0.66	1.57	5.45	4.32	10.5	1.14	0.5	0.91	6.30	5.4	0.01
Ba	27	750	130	3.9	520	2730	460	360	750	133	830	1800	1400	12
La	1.1	0.48	2.8	19.6	23.2	11.3	21.1	10.7	11.4	21	2.5	40	35	0.64
Ce	2.0	2.0	7.0	19.6	23.2	34.8	35.2	24.2	20.9	32.1	5.0	75	62	3.0
Nd	0.7	<1	4.0	15.4	21.9	19.4	18.2	13.8	9.2	12.2	3.0	27	26	<0.5
Sm	0.19	0.12	0.91	2.3	4.01	3.12	3.52	3.08	1.85	2.12	0.28	2.5	3.1	0.12
Eu	0.03	0.20	0.20	0.50	0.62	0.72	0.94	1.01	0.31	0.44	0.10	0.80	0.8	0.05
Gd	n.d.	n.d.	n.d.	2.5	3.1	3.5	3.4	3.1	0.85	0.92	n.d.	n.d.	n.d.	n.d.
Tb	0.03	0.05	0.74	0.43	0.53	0.61	0.51	0.53	0.13	0.16	0.06	0.45	0.50	0.04
Dy	0.31	0.34	4.3	2.6	3.05	4.1	3.1	3.1	0.66	0.95	0.3	2.6	2.8	0.12
Tm	n.d.	n.d.	n.d.	0.19	0.22	0.37	0.24	0.23	n.d.	n.d.	n.d.	n.d.	n.d.	n.d.
Yb	0.13	0.50	5.00	1.30	1.37	2.72	1.54	1.45	0.4	0.56	0.25	3.00	3.00	0.06
Lu	0.02	0.06	0.50	0.18	0.17	0.41	0.24	0.2	0.057	0.095	0.04	0.40	0.40	0.01
Hf	0.07	0.20	3.30	3.49	4.73	8.01	2.71	1.92	2.14	1.12	0.20	5.0	3.0	0.3
Ta	0.01	0.36	0.33	0.62	0.38	1.09	0.42	0.11	0.46	0.2	0.01	0.51	0.33	0.04
W	0.51	<0.3	0.43	0.6	0.53	0.69	0.58	0.64	2.7	0.9	0.5	0.68	0.58	0.28
Ir (ppb)	<0.6	<0.6	<1	<0.6	<0.8	<0.5	<1	<1	<0.5	<0.9	<0.6	<1	<1	<0.6
Au (ppb)	0.7	3.4	1.7	2.3	1.6	0.2	1.1	0.8	5.5	1	<0.9	3.6	4.3	0.6
Th	0.21	1.4	8.5	11.8	12.2	65.9	9.53	1.66	17.7	9.68	1.3	38	22	0.5
U	0.12	0.33	1.4	1.95	1.12	9.78	1.83	1.02	1.15	4.55	0.55	2.5	2.1	<0.06
K/U	14508	45972	12494	19046	29533	3094	11325	27958	44333	1403	34064	34088	40305	
Zr/Hf	185.71	105.00	38.18	27.22	15.01	23.85	36.16	40.63	35.51	87.50	95.00	39.80	41.33	86.67
Hf/Ta	7.00	0.56	10.00	5.63	12.45	7.35	6.45	17.45	4.65	5.60	20.00	9.80	9.09	7.50
La/Th	5.24	0.34	0.33	1.66	1.90	0.17	2.21	6.45	0.64	2.17	1.92	1.05	1.59	1.28
Th/U	1.75	4.24	6.07	6.05	10.89	6.74	5.21	1.63	15.39	2.13	2.36	15.20	10.48	
LaN/YbN	5.72	0.65	0.38	10.19	11.44	2.81	9.26	4.99	19.26	25.34	6.76	9.01	7.88	7.21
Eu/Eu*	0.491	3.362	0.321	0.637	0.537	0.666	0.830	0.999	0.755	0.963	0.995	0.988	0.837	0.953

Major element data (in wt.%) by XRF; L.O.I. = loss on ignition at 1100°C; all Fe as Fe_2O_3; Trace elements (in ppm, except as noted): V, Cu, Y, and Nb by XRF; Ni, Zr, and Sr: INAA and XRF data; all others by INAA; some values are averages of replicate determinations.

SAMPLES AND ANALYTICAL PROCEDURES

Sampling localities for the sample collection of REIMOLD and MILLER (1989) and this study are shown in Fig. 4, which also presents a schematic map of the crater geology. Detailed petrographical descriptions of newly analyzed samples are given in the Appendix. A detailed account of target rocks and breccias is given by REIMOLD and MILLER (1989). Figures 5 and 6 present microphotographs of some of the new samples (designated URK-): calcareous sandstone 73A (Fig. 5a), quartzitic melt breccia 87A (Fig. 5b), a mylonitic autochthonous breccia from within the granitic rim basement (81A, Fig. 5c), as well as various types of melt breccias and selected clasts therein (Figs. 5d–f, 6a–c). Samples 86A (Fig. 6d,e) and 86C* are unique among the Roter Kamm sample suite. Both specimens occur as rounded clasts within schistose melt breccias and are mineralogically very similar. They consist entirely of mica, pyrite, chlorite, and minor plagioclase and quartz.

Major element analyses were done by standard X-ray fluorescence (XRF) procedures, on powdered aliquots from samples weighing between 0.5 and 1 kg for country rocks and 100–200 g for breccias. Precision and accuracy (as determined by standard and duplicate sample analysis) are similar at (in wt%) about 0.4 for SiO_2, 0.03 for TiO_2, 0.2 for Al_2O_3 and MgO, 0.1 for Fe_2O_3, CaO, and K_2O, 0.01 for MnO and P_2O_5, and 0.3 for Na_2O. The concentrations of V, Cu, Y, and Nb were also determined by XRF analysis (accuracy 0.5–1, 0.5–1, 1–1.5, and 0.5–1 ppm, for low to high concentrations, re-

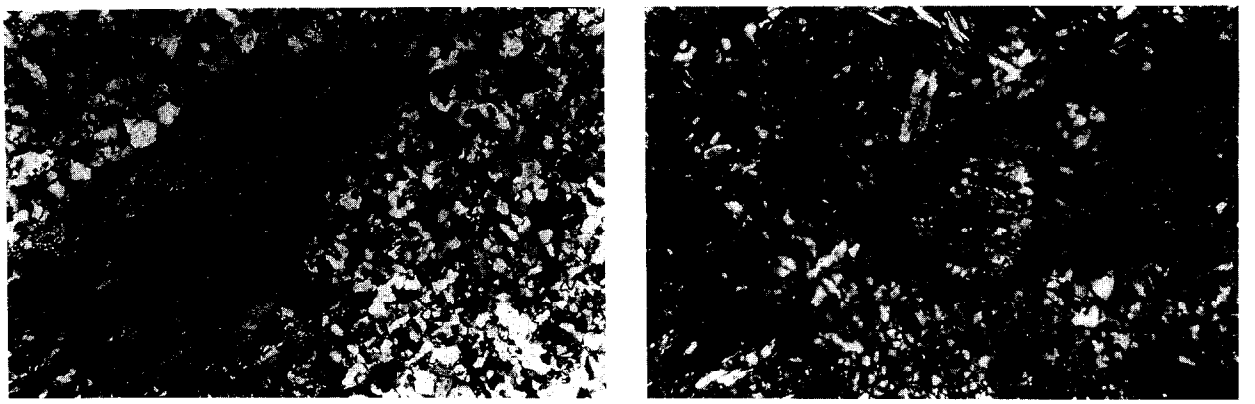

FIG. 6. Photomicrographs of melt breccias and of vesicle filling within melt breccia: (a) quartzitic melt breccia 68* with partially oxidized and fused (upper part) shale clast (crossed nicols, width: 2.2 mm); (b) schistose melt breccia 92A with quartz clast (center) displaying shock mosaicism and annealed melt or diaplectic quartz glass (dark band running N–S) (crossed nicols, width: 720 μm); (c) bottom half of clast of Fig. 7b with planar features (arrow) in relic grains (crossed nicols, width: 220 μm); (d) 86A—vesicle filling: Marginal zone with mica and pyrite crystals set into chlorite matrix (crossed nicols, width: 2.2 mm); (e) 86A—central zone composed of large mica flakes, some pyrite, and minor plagioclase (in between pyrite, center) and quartz (crossed nicols, width: 2.2 mm).

spectively). All other trace elements were analyzed by instrumental neutron activation analysis (INAA) following procedures described by KOEBERL et al. (1987) and KOEBERL (1993). For most samples, Sr and Zr concentrations were determined by both XRF and INAA, and for some of the low abundance samples, Ni data were also obtained by XRF.

RESULTS AND DISCUSSION

Target Rocks

The target geology of the Roter Kamm crater comprises a large variety of different rock types. Table 1 gives the abundances of forty-seven chemical elements as well as some geochemical parameters for fourteen target rock samples. The total database for all samples (target rocks and breccias) from REIMOLD and MILLER (1989) and from this study is presented in the ternary diagrams of Figs. 7a,b (major element abundances) and 8a,b (CIPW normative mineral proportions). Both the metamorphic and magmatic target rocks of the Namaqualand Metamorphic Complex as well as the overlying Gariep metasedimentary rocks display a broad compositional range. Samples from the Namaqualand Metamorphic Complex basement have moderate to high concentrations of Ba, Rb, Hf, Ta, As, Cs, U, Th, Sc, and of siderophile elements. They can be discriminated from the group of pegmatite samples by higher Hf, Ta, As, Sc, and U contents. The metasediments analyzed to date (44A, 73A, 35*, 79*, 9/9A*) show abundances similar to those of the granitic basement rocks (Table 1).

As one of the objectives of our study was to better define the pegmatite-derived quartz-feldspar component of the target rocks, we report here three new analyses of pegmatite samples (Table 1). These are the slightly deformed specimens 123 and 75 as well as monomict breccia 83 (see Appendix). Previously, only one pegmatite (7A*) and one pegmatitic pseudotachylite (72A*) had been analyzed. Figure 7a,b indicates significant chemical differences among the now available pegmatite data for most major elements. However, as shown in Fig. 8a,b, this appears to be primarily the result of variable quartz contents. As the quartz veins and quartz-feldspar pegmatites intruding the rim are very coarse-grained, even kilogram sized samples may not be representative. The wide variety of pegmatite compositions does not favor further mixing calculations with the aim of determining possible contributions of pegmatite facies to the composition of any melt breccia.

Chondrite-normalized (HASKIN et al., 1968) rare earth element (REE) patterns are shown in Fig. 9a. Pegmatite samples 75, 83, and 123 have lower REE concentrations than the orthogneisses and granites of the Namaqualand basement from the Roter Kamm area. In agreement with their mineralogy, they have variable Eu signatures: sample 75 (high plagioclase content) shows a distinct positive anomaly, 83 (contains both plagioclase and microcline as minor components) shows no anomaly, and 123 (little K-feldspar and plagioclase, some muscovite) is characterized by a slight negative Eu anomaly. Other pegmatite samples analyzed earlier show similar REE concentrations and patterns (samples 7A* and 52B/P*; Fig. 15b in REIMOLD and MILLER, 1989).

Granite 85 and orthogneiss 38 are enriched in heavy REEs (HREEs) and display a pronounced negative Eu anomaly. In these respects these two samples are rather unusual among the Namaqualand basement samples from Roter Kamm (compare Fig. 15a in REIMOLD and MILLER, 1989). The mylonitic to pseudotachylitic samples 81A and 81B from K-feldspar–rich granitic basement display light REE (LREE) enriched patterns without pronounced Eu anomalies that closely resemble those for 31B and 39 orthogneiss and breccias (Fig. 9c). Contrary to this, K-feldspar-rich granite 24* (REIMOLD and MILLER, 1989) displays the largest negative Eu anomaly determined for a Roter Kamm basement rock.

Orthogneiss breccias 81A and 81B, separated from the same host rock sample, are of very similar composition. The differences observed for several elements (Table 1) may reflect the somewhat heterogeneous composition of the coarse-grained host rock (e.g., feldspar and biotite abundances are variable on a centimeter scale). However, compared to the

FIG. 6. (Continued)

general composition of the granitic-granodioritic NMC basement (as exemplified by data for samples 8*, 17*, 18*, 24*, and 34*), samples 81A and 81B do not indicate admixture of another basement rock component. Samples 81A and 81B are also very similar in composition with regard to the REEs, indicating that the formation of cataclastic or mylonitic breccias as well as of pseudotachylites took place under isochemical conditions. The fact that samples 81A and 81B show nearly identical patterns does not favor the possibility that fluids played a significant role during the pseudotachylite-forming process (unless the REE concentrations in these two samples were completely overprinted by later hydrothermal processes which contradicts petrographic evidence).

Four aplite samples have by now been analyzed from the Roter Kamm collection: samples 24* and 34* from MILLER and REIMOLD (1986) and samples 21 and 38B from this study. Although some variation in total REE contents is apparent (Fig. 9b), shapes and slopes of all four patterns are rather similar. Considering the trace element data for 24* and 34* (REIMOLD and MILLER, 1989), the aplites are not distinctly different from other basement rocks.

Melt Breccias

Several varieties of melt breccias were described by REIMOLD and MILLER (1989). The most common variety displays evidence for local melting or has the texture of a partially recrystallized schistose rock. These melt breccias were collected at a locality on the north-northwest part of the crater rim and were described by REIMOLD and MILLER (1989) as similar to the pancake-like "flädle" known from the Ries crater in Germany, and were accordingly classified as "ejected breccias." These samples all consist mainly of coherent to locally brecciated, well-foliated, and strongly folded schist with angular fragments ranging from millimeter to centimeter in size. Melting is restricted to individual submillimeter to several millimeter wide bands or small elongated lenses. Some samples of this type contain rare fragments of quartzite (or annealed pegmatite- or vein-derived quartz) and even of granitic basement. It may also be significant that small clasts of this same schist lithology were occasionally observed in pseudotachylitic breccias hosted by quartz- (or quartz-feldspar-) pegmatite (the so-called "black-and-white" breccia of DEGENHARDT et al., 1992, 1994). Due to the lack of a better term and because such breccias are not known from other impact craters, this group of melt breccias was termed "schistose" melt breccias (REIMOLD and MILLER, 1989; KOEBERL et al., 1990a).

Several other, previously analyzed melt breccia samples (30*, 41*, 68*) have petrographic characteristics and chemical compositions that are distinctly different from the "schistose" melt breccias. Breccia 41* is important because it contains glass that was used for ^{40}Ar-^{39}Ar dating (KOEBERL et al., 1993), as well as quartz and granite clasts that show characteristic shock deformation features (REIMOLD and MILLER, 1989); it is thus a "true" impact melt breccia formed due to shock melting. A third type of melt breccia is texturally very similar to the schistose melt breccias, but contains significantly more silica at the expense of sericite and iron oxides. Locally these breccias also appear to have been melted (fine-grained recrystallized patches), and, consequently, they have been classified as "quartzitic" melt breccias. As both schistose and quartzitic melt breccias were collected at the same site on the northern crater rim, and as the schistose melt breccias often show alternating laminae of schist and quartzite on a microscopic scale, we conclude that this target lithology (Gariep schist and quartzite) was heterogeneous and composed of alternating and intercalating schistose and quartzitic layers or lenses.

The limited compositional variability of schistose melt breccias is evident in Figs. 7a,b and 8a,b. A melt breccia containing only quartz and quartzitic inclusions (87A) analyzed in the course of this study was found to be texturally

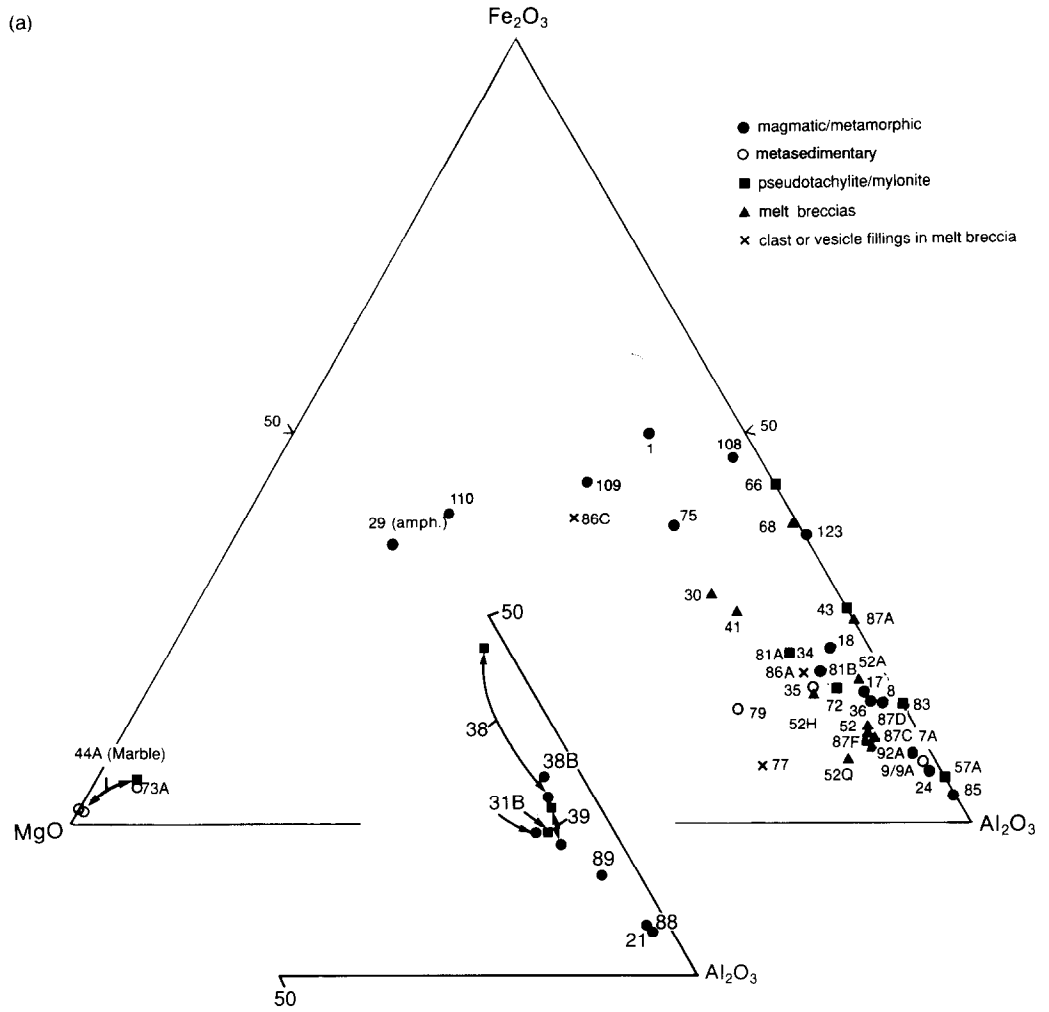

FIG. 7. Major element compositions of all Roter Kamm samples analyzed to date, in terms of (a) Fe_2O_3-MgO-Al_2O_3 and (b) K_2O-CaO-Na_2O. Arrows connect breccia-host rock pairs. Part of the new data have been plotted separately (inset) to avoid superposition of data for Al_2O_3-rich samples.

and chemically very similar to 68*. However, some mixing of schist with pegmatite-derived material has been indicated, and is further supported by the occurrence of a few melt breccia clasts in calcrete samples that were collected on the outer base of the crater rim and contain fragments of coarse-grained (up to 0.7 cm) quartz-pegmatite (see below). CaO and MgO contents of schistose melt breccias are rather low (0.2 and 0.4 wt%, respectively), which precludes a significant contribution from Gariep marble.

The schistose melt breccias have K_2O/Na_2O ratios generally much higher than most of the available parent rock lithologies (Table 1-3; REIMOLD and MILLER, 1989). The newly analyzed schistose melt breccias and the pseudotachylite samples (see below) have similarly high ratios. Schist sample 79* (Table 2 in REIMOLD and MILLER, 1989) has a K_2O/Na_2O ratio of 93, which is about 6–45 times higher than the ratios calculated for schistose melt breccias. Thus, mixing of schist, quartzite, and pegmatite could explain the elevated alkali element ratios.

All samples, independent of their origin from either mainly schist or from mixed parent rocks (e.g., 41*), display similar interelement ratios. The schistose melt breccias as a group show a limited compositional variability for elemental abundances as well as interelement ratios (Table 2). They are characterized by, e.g., high U, V, Ba, and W, and low Co and Sr abundances. Characteristic differences in chemical composition exist between the schistose breccias (89C, 87D, 87F, 92A, 52A*, and 52Q*), the quartzitic melt breccias (52B/M*, 87A), and the "true" impact melt breccias (41*, 68*). Apart from most major element concentrations (e.g., Al, Ti, Mg, Ca, K), the abundances of many trace elements vary significantly between these three breccia types. For example, the concentrations of Sc, V, Zn, Ga, Rb, Sr, Zr, Ba, Hf, Ta, Th, and especially U are different in schistose breccias by a factor of about 2–20 compared to those in the quartzitic breccias (Table 2; Table 3 in REIMOLD and MILLER, 1989). Such a difference exceeds by far the difference in SiO_2 content and is related to different source materials. While distinct in composition from the other melt breccia types, the "true" impact melt breccias 41* and 68* are more heterogeneous and show the chemical contribution of their various lithologies, especially granite. Breccia 52A* contains a single gra-

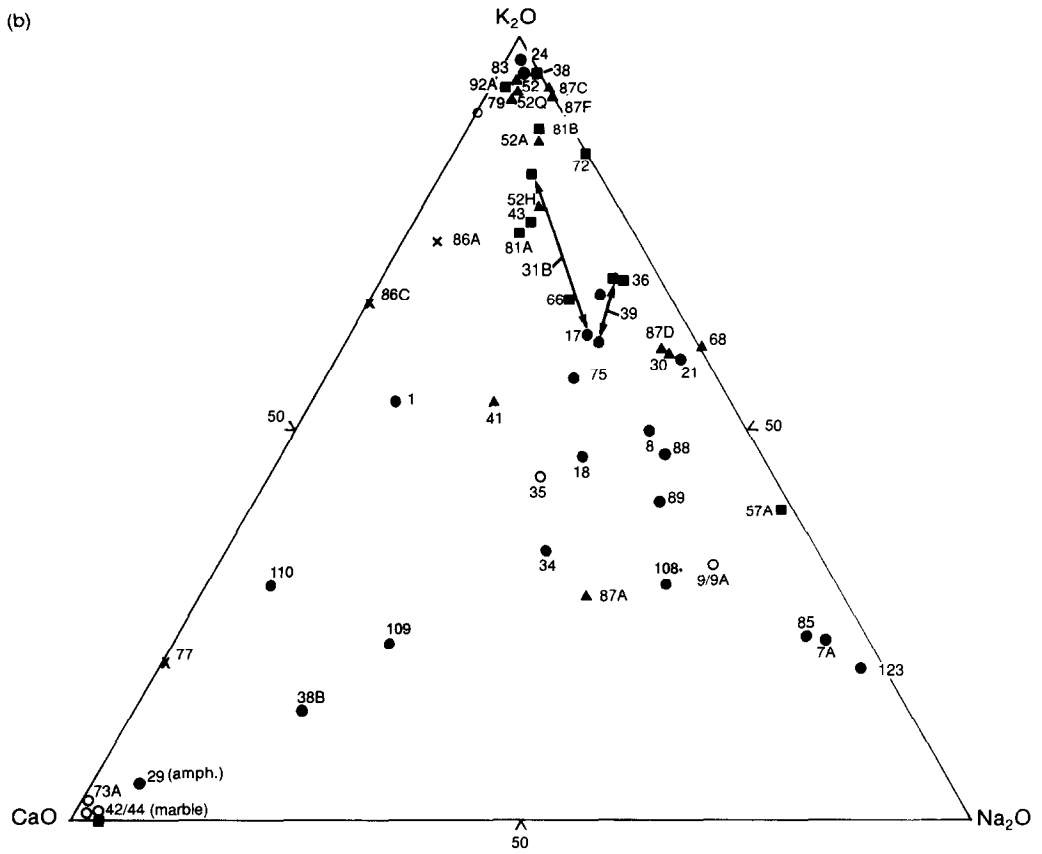

FIG. 7. (Continued)

nitic clast. Together with the observation that some melt breccia clasts in calcrete probably contain pegmatite-derived inclusions, there is reasonable evidence for limited mixing between schist, quartzite, granite, and pegmatite.

The schistose melt breccias also show a very narrow range in REE concentrations and have essentially identical REE patterns (Fig. 9d). They are also clearly distinct from the quartzitic breccias 52B/M* and 87A (Table 2; Fig. 9d; Table 3 in REIMOLD and MILLER, 1989; the high Sm value for 52B/M* may be due to an analytical problem in the earlier work). The REE patterns also indicate that the schistose and quartzitic melt breccias from the Roter Kamm impact crater were derived from different parts of a stratigraphic unit with internally variable quartzite-schist proportions. The limited range in REEs and other trace element concentrations in the schistose melt breccias indicates that they were derived from a uniform and well-defined source rock, in contrast to the other melt breccias which show more variability.

In agreement with REIMOLD and MILLER (1989), we do not observe any siderophile element enrichments in any of the Roter Kamm melt breccia types. No Ir was detected in the melt breccias above our detection limit of 0.5–1 ppb. The high Cr contents of most melt breccias can be related to the composition of main precursor rock types (metasediments and crystalline basement), as they are not accompanied by high Co or Ni values (Tables 2 and 3, and REIMOLD and MILLER, 1989) that would be expected from a meteoritic component. A high Cr content (720 ppm) was found also for schist sample 79*.

During the most recent field trip to Roter Kamm, several exposures of fine- to medium-grained micaceous gneisses belonging to the NMC basement were observed on the western part of the crater rim. As the surface below these exposures was covered with chips and small boulders resembling the schistose melt breccias, several samples (108–110) were collected and analyzed (Table 1). However, the results show that the schistose melt breccias are not related to this texturally similar NMC material. Erosion, wind-ablation, and sand-blasting are likely to be responsible for the shapes of these schist samples.

None of the target rocks analyzed so far (REIMOLD and MILLER, 1989; Table 1) has a composition that is identical or closely similar to that of the schistose melt breccias. Only for some of the other melt breccias, for example, sample 41*, a contribution from basement material has been verified by the identification of granitic clasts (REIMOLD and MILLER, 1989). Recently, a small area on the north-northwest part of the rim, where the schistose breccias were found, was excavated (thanks to the physical efforts of M. Zolensky and P. Jakes). It seems as though the scattered occurrences on the surface lead to a large solid, subsurface body of schistose material. This new field evidence, together with the chemical data given above, require a new interpretation of these breccias, in contrast to REIMOLD and MILLER (1989). The shapes

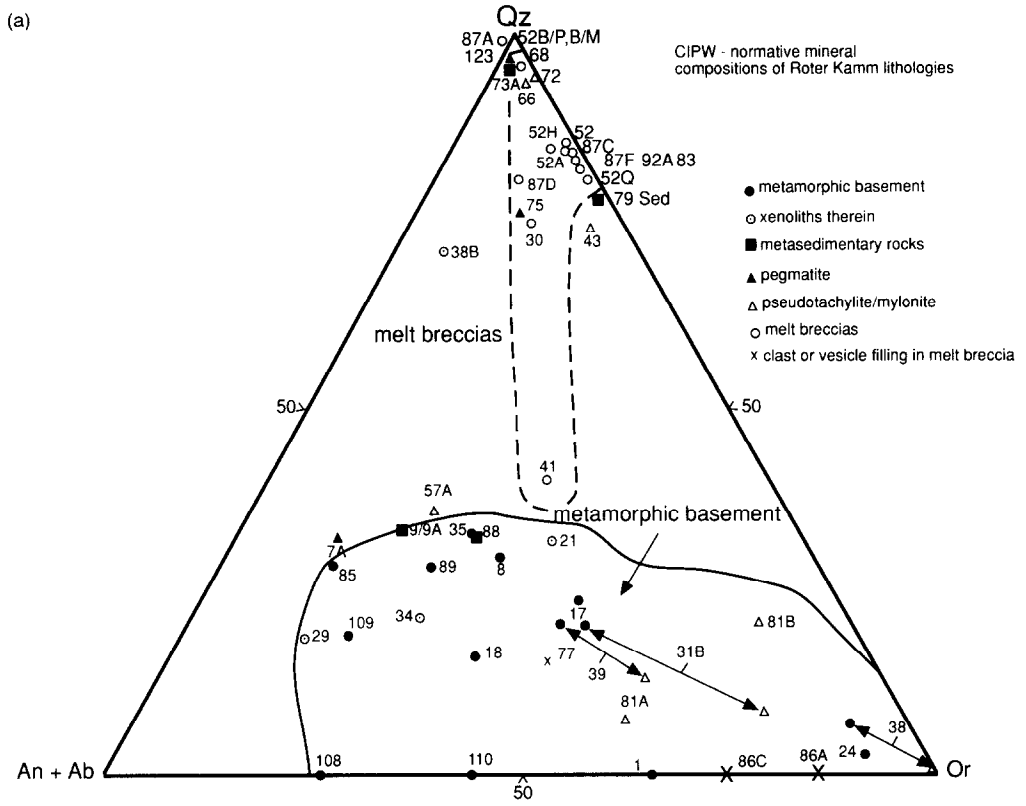

FIG. 8. CIPW normative mineralogy of Roter Kamm samples: (a) normative quartz-plagioclase (An + Ab)-orthoclase abundances; (b) normative quartz-total feldspar-pyroxene ± olivine abundances. Abbreviations as in Fig. 7.

and surface characteristics, previously thought to be due to ablation or "splash-forms" of molten rock, similar to the "flädle" at the Ries crater, are more easily explained by erosion from the abrasive action of wind-blown sand. They have been derived from a confined body of schist as part of the Gariep metasediments that were overlying the NMC basement at the time of the impact. We now conclude that the schistose melt breccias have formed in situ and only show limited melting (maybe by frictional melting) on a local scale, and that they are not ejected melt breccias.

Clasts in Calcrete

To study the possible variety of the target rocks, we examined the clast population in two calcrete specimens from the outer base of the crater rim (Figs. 4, 10a). In the size range from 3 mm to >25 mm, about one quarter of the schistose melt breccia clasts in calcrete contains single coarse-grained quartz or quartzitic inclusions, most of which are probably derived from quartzite or sandstone of the upper stratigraphic zone. The presence of such melt breccia clasts together with other types of inclusions observed in calcrete, such as quartzite, quartz, jasper or marble, and schist, also indicates that much of the clastic component is derived from metasedimentary Gariep strata. The few identified pegmatite clasts basically represent the only component of igneous origin; only two granite or gneiss inclusions were found among the 254 clasts identified.

In addition to the determination of the macroclast population, 590 and 415 microclasts in the size range from ~70 μm to 3 mm were identified in thin sections of these two calcrete samples, respectively (Fig. 10b–e). Again the large majority of inclusions originates from sedimentary lithologies. The total percentage of clasts that could have been derived from crystalline basement lithologies amounts to <5 and <4.3% in these two samples (excluding the quartz clast component), as compared with >30% of clearly identified metasediment-derived clasts. In sample URK-C1, a single shocked quartz clast with planar deformation features was identified (Fig. 10b). Some quartzitic and schistose melt breccia microclasts were also observed in the two calcrete samples. Several other clasts, in particular a granitic inclusion, show evidence for partial fusion. Other quartz clasts show strong strain deformation such as narrow deformation bands, subplanar fluid inclusion trails, or undulatory extinction. These effects, previously described from some pseudotachylitic breccias (REIMOLD and MILLER, 1989), could be attributed to the impact event as well, but per se do not represent characteristic shock deformation.

The shapes of most quartz and quartzitic clasts are subangular to slightly rounded. However, the identified schistose melt breccia clasts, as well as the schist and siltstone clasts, are well rounded, often displaying oval shapes. The observation that many melt fragments found within the calcrete have abraded shapes could indicate that the melt clasts are erosional debris fragments from the crater rim. This can also

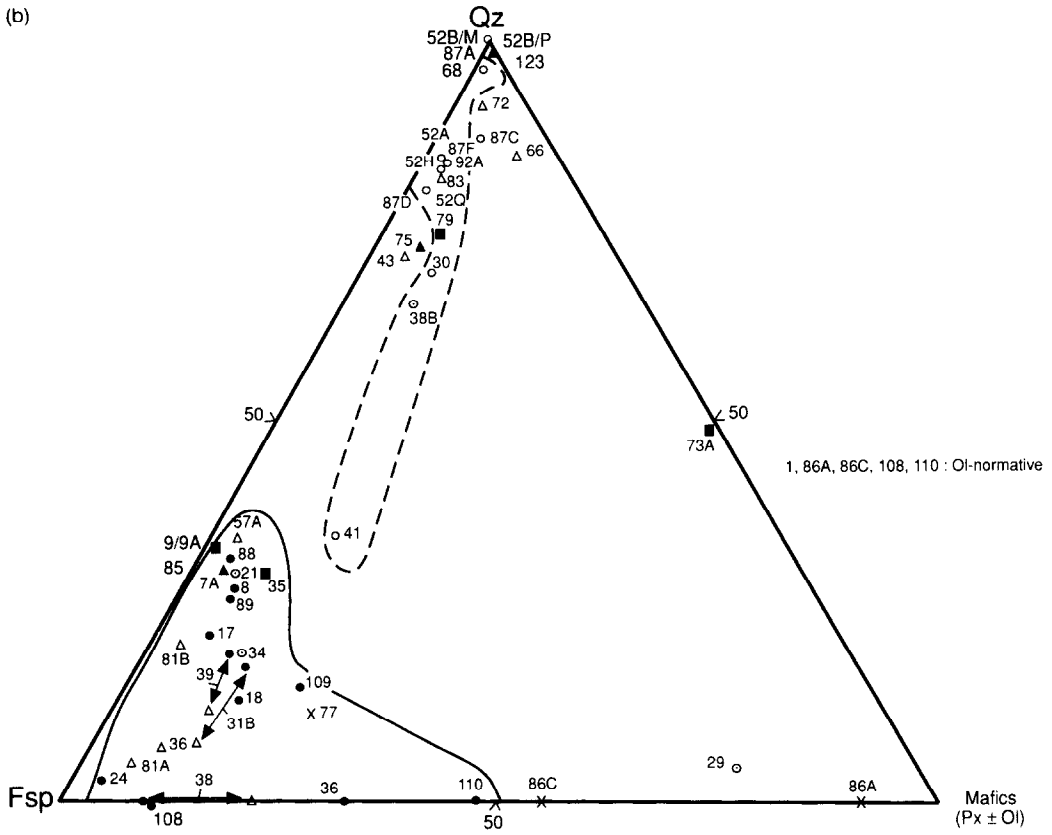

FIG. 8. (Continued)

be used to constrain the age of the crater: the cratering event must have taken place during or just after deposition of the calcrete. The calcrete is a hard pan that may be equivalent to the End-Miocene calcrete of the central Namib desert which was estimated at ca. 5 Ma (e.g., STOCKEN, 1978; WARD et al., 1983; WARD, 1987). As the crater age is well constrained at 3.7 ± 0.3 Ma (KOEBERL et al., 1993), the previous age estimate for this particular calcrete seems somewhat too high.

Host Rock/Breccia Pairs

Compositions of several pseudotachylitic or mylonitic breccias and their host rocks (31B, 38, 39, and 44A; Table 3) were studied for differences and alteration effects. The host-rock-normalized abundances for the four breccias are shown in Fig. 11a (major elements) and b (trace elements). Analyses of the orthogneiss and mylonite in the sample pair 31B show an enrichment of Fe_2O_3 and K_2O and a depletion of Na_2O in the breccia. This could be due to slight compositional variation of the host rock or reflect preferential melting of K-feldspar and ferromagnesian minerals which has also been observed at other pseudotachylite localities (e.g., MADDOCK, 1986, 1992; REIMOLD, 1991).

Pseudotachylite 38-PT shows a strong Fe_2O_3 enrichment and depletions of MnO and MgO. Some differences could be due to alteration. Secondary quartz veinlets and appreciable amounts of chlorite were observed in samples 38-HR and 38-PT. Alteration may also have contributed to the chemical differences between samples 31B-HR and 31B-Myl. Most biotite and hornblende is found to be entirely converted to either Mg- or Fe-rich chlorites. Sample 39-PT shows some K_2O and Na_2O enrichment and otherwise a pattern that is similar to sample 38-PT. The differences in alkali abundances may be due to sericitisation of feldspar in these samples. Where the host rock to pseudotachylitic or mylonitic breccia is orthogneiss (31B, 38, 39), distinct enrichments in normative orthoclase content are found (Fig. 8a), accompanied by a decrease in normative quartz content or increase in the mafic component of the breccias (Fig. 8b). The differences are most pronounced for marble sample 44A-PT with an almost general enrichment in most elements (Fig. 11a), especially for Al_2O_3, MnO, and K_2O. Some differences can be explained by the mineralogical heterogeneity of the host marble with respect to quartz and (Fe,Mn)-oxide contents.

The host-rock-normalized patterns for the trace elements (Fig. 11b) are consistent for the three orthogneiss datasets (samples 31B, 38, and 39) which show a parallel trend. Sample 31B-Myl shows minor enrichments for Rb, Sb, and Cs, a strong enrichment for As, and strong depletion for Cr. Sample 38-PT shows also an enrichment in As and a depletion of Ta, Sc, and Cr, which could be explained by slight variation in the abundance of mafic minerals of the parent rock. Sample 39-PT displays a significant enrichment in As. For marble

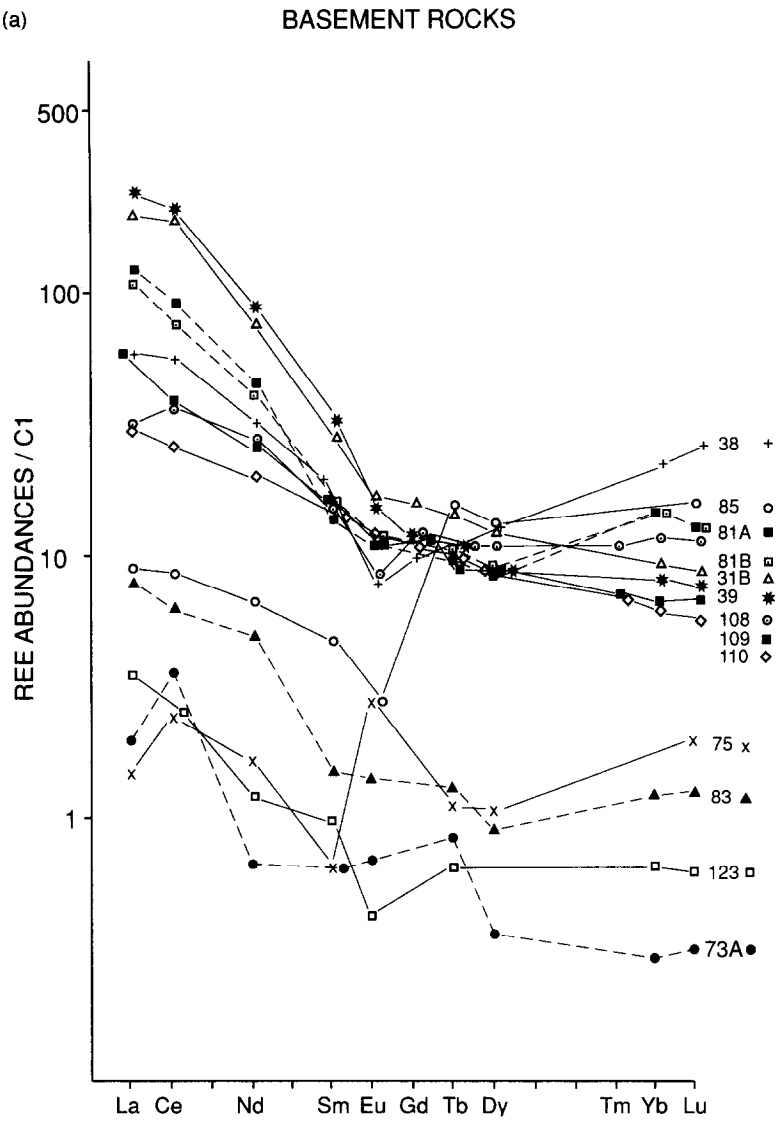

FIG. 9. Chondrite-normalized (HASKIN et al., 1968) rare earth element (REE) patterns for newly analyzed Roter Kamm samples, as well as for all Roter Kamm aplites analyzed to date: (a) basement rock samples and associated mylonitic or pseudotachylitic breccias; (b) REE abundances for the four aplitic samples; (c) melt breccias and vesicle filling 86A; (d) country rock-pseudotachylite/mylonite pairs.

samples 44A most trace elements are also found to be considerably enriched in the breccia. This result has already been explained by the variable composition of the Gariep marble. It should also be noted here that the about 3 cm wide pseudotachylite vein, from which sample 44A was obtained, extends over at least 100 m. This could indicate that at least some lateral mixing or variation could have occurred within this extensive vein.

REE patterns of host rock-breccia pairs (Fig. 9d) present two main results: In all four cases the corresponding patterns for host rock and breccia resemble each other closely. Obviously no REE fractionation occurred upon breccia formation. However, the 38 and 31B breccias show lower absolute concentrations than their host rocks, while for 39 and 44A this trend is reversed. In the case of marble sample -44A this could again be explained by precursor rock heterogeneity. Inconsistent trends for REE behavior on pseudotachylite formation in felsic, intermediate, and mafic environments were also noted for Vredefort pseudotachylites (REIMOLD, 1991).

Monomict breccias within granitic host rocks all display the chemical characteristics of the basement rocks. It is not immediately obvious whether mixing of several basement rock types played a role in the formation of pseudotachylite. However, individual analyses (e.g., sample 66*) show that patterns within the overall group vary significantly. This probably supports the suggestion of REIMOLD and MILLER (1989) that limited mixing between granitic and pegmatitic components could be a factor. The results also shed new light onto the problem of whether hydrothermal effects accompany the formation of mylonitic and pseudotachylitic breccias. Strong enrichments or depletions of some mobile elements, such as Ga, As, Se, Rb, Sc, Cs, or Ta, indicate that some

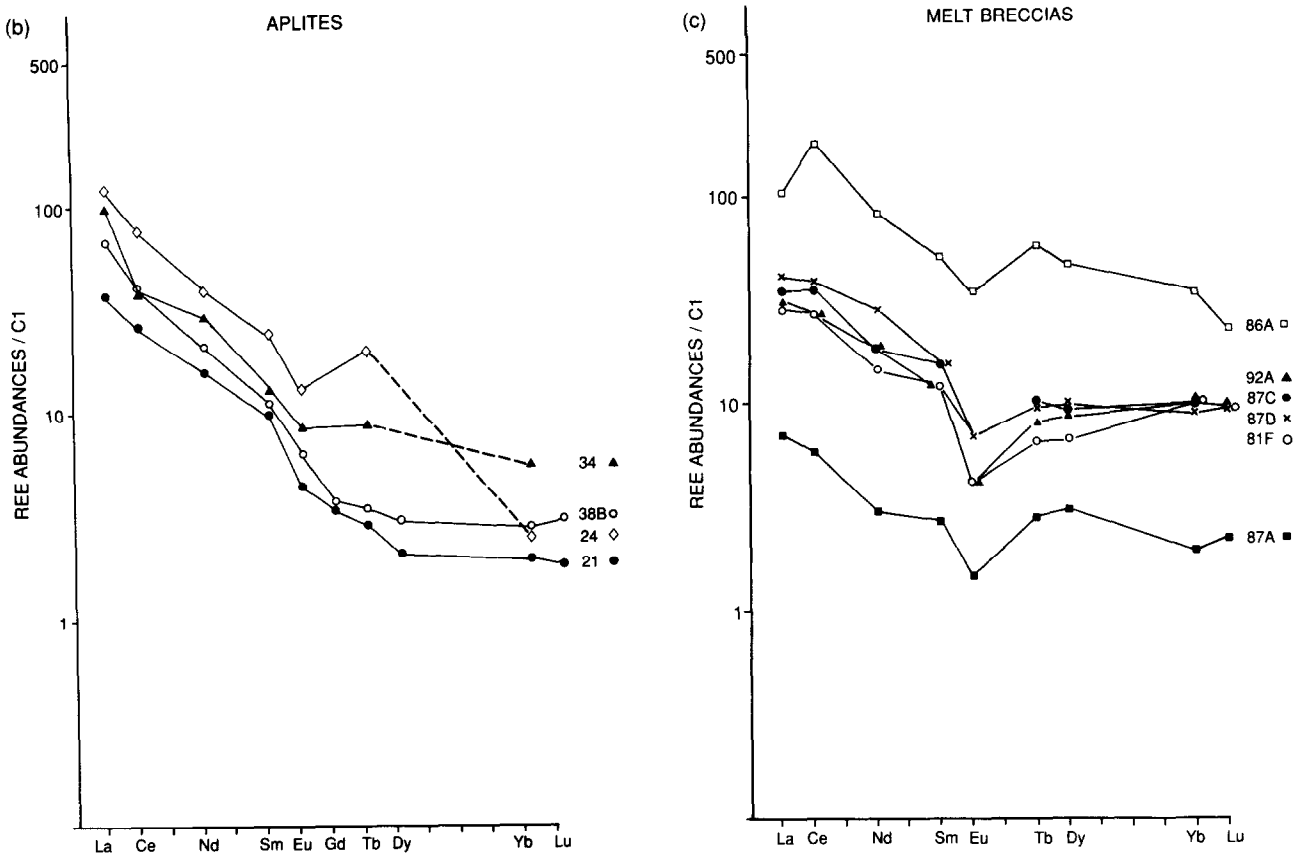

COMPARISON OF PSEUDOTACHYLITIC / MYLONITIC BRECCIA - HOST ROCK PAIRS

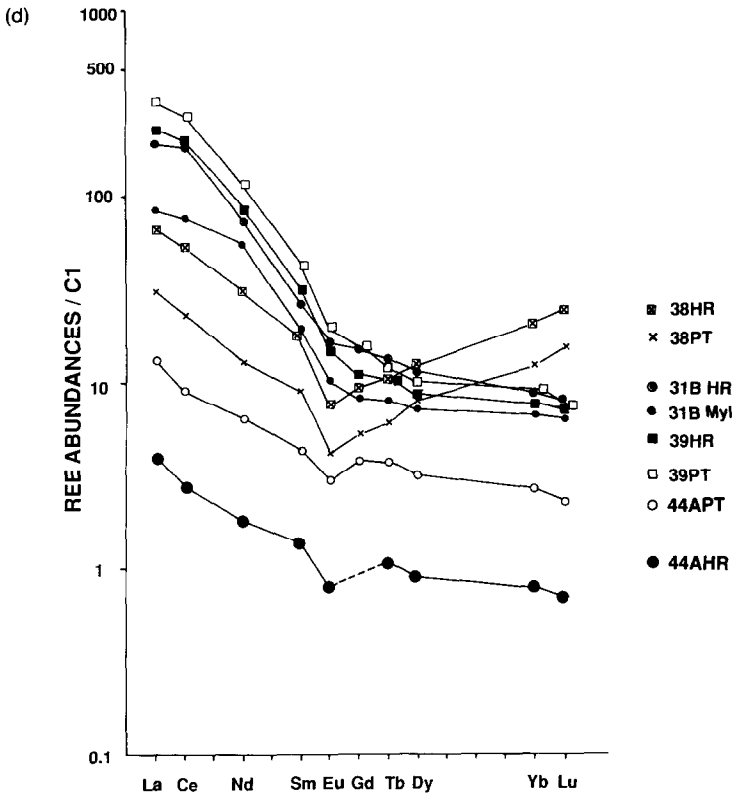

FIG. 9. (Continued)

TABLE 2. MAJOR AND TRACE ELEMENT COMPOSITION OF MELT BRECCIAS FROM THE ROTER KAMM IMPACT CRATER.

	87A	87C	87D	87F	92A	86A
SiO_2	96.19	89.71	90.54	89.51	88.31	47.23
TiO_2	0.01	0.32	0.27	0.29	0.37	1.12
Al_2O_3	1.20	4.83	4.13	4.96	5.29	26.07
Fe_2O_3	0.42	0.60	0.56	0.59	0.61	6.94
MnO	0.02	0.04	0.02	0.02	0.02	0.17
MgO	0.01	0.36	0.33	0.37	0.43	4.23
CaO	0.21	0.04	0.11	0.06	0.08	3.06
Na_2O	0.26	0.11	0.92	0.13	0.13	0.54
K_2O	0.18	1.73	1.51	1.82	1.93	10.04
P_2O_5	0.01	0.03	0.02	0.03	0.04	1.42
L.O.I.	0.91	1.97	2.17	1.81	2.44	0.01
Total	99.42	99.74	100.58	99.59	99.65	100.83
Sc	0.48	5	4.3	4.8	5.1	26
V	21	117	106	115	126	346
Cr	189	196	214	180	238	93
Co	1.2	0.62	0.75	0.9	0.78	17
Ni	2.4	3	2.4	3.6	4.5	56
Cu	<2	<2	<2	<2	<2	<2
Zn	5	17	13	16	16	120
Ga	2.6	15	13	15	15	49
As	0.7	0.5	0.4	0.6	0.3	0.5
Se	0.9	1.3	<0.1	1	<0.1	1.2
Br	<1	0.2	<0.5	<0.5	<0.5	<0.5
Rb	9	80	70	90	80	420
Sr	34	4.4	1.4	6.5	5.8	74.6
Y	8.6	20.4	18.3	20.6	22.8	75
Zr	15	82	69	78	88	266
Nb	1.2	8	6	7.7	9.2	7.7
Sb	0.16	0.22	0.15	0.14	0.16	0.49
Cs	1.8	0.91	0.78	0.97	1.00	4.00
Ba	60	1000	950	900	1100	1600
La	2.2	11	13	9.2	9.9	33
Ce	4	29	32	22	22	150
Nd	1.8	11	17	8.6	11	49
Sm	0.51	3.00	2.9	2.3	2.3	9.7
Eu	0.1	0.4	0.5	0.3	0.3	2.5
Gd	n.d.	n.d.	2.4	n.d.	n.d.	n.d.
Tb	0.13	0.47	0.46	0.35	0.38	2.7
Dy	0.98	3.0	3.1	2.5	2.8	15
Tm	n.d.	n.d.	0.28	n.d.	n.d.	1.1
Yb	0.4	2.0	1.8	2.0	2.1	7.0
Lu	0.07	0.3	0.3	0.3	0.3	0.7
Hf	0.1	2.0	2.0	2.0	2.0	8.5
Ta	<0.02	0.49	0.41	0.51	0.51	0.41
W	0.7	4.4	3.2	4.2	3.5	4.7
Ir (ppb)	<1	<1	<1	0.9	<1	0.04
Au (ppb)	1	0.1	<0.3	0.9	0.1	0.1
Th	0.41	5.8	6.7	4.9	6.4	24.0
U	0.26	20	18	13	16	1.9
K/U	5739	717	695	1161	1000	43806
Zr/Hf	150.00	41.00	34.50	39.00	44.00	31.29
Hf/Ta		4.08	4.88	3.92	3.92	20.73
La/Th	5.37	1.90	1.94	1.88	1.55	1.38
Th/U	1.58	0.29	0.37	0.38	0.40	12.63
LaN/YbN	3.72	3.72	4.88	3.11	3.19	3.19
Eu/Eu*	0.510	0.438	0.579	0.429	0.413	0.627

See Table 1 for further notes.

hydrothermal alteration may have taken place. However, it is not clear when this alteration occurred relative to breccia formation.

Impact-Induced Hydrothermal Alteration

Some rare quartz pebbles that were found on the crater rim have unusual characteristics, leading KOEBERL et al. (1989, 1990a,b) to propose that they have formed in an impact-induced phase of hydrothermal activity. The presence of the unusual clasts 86A and 86C* hosted by schistose melt breccias provide additional evidence for this hypothesis. The composition of 86A (Table 2) is unique among Roter Kamm samples and also deviates somewhat from that of sample 86C* (REIMOLD and MILLER, 1989), which is thought to be of the same origin. When the individual mineralogical compositions are considered, however, this difference is readily explained by the variable ratios of light mica to chlorite, which is much higher for sample 86A. The mineralogical composition of both clasts is dominated by minerals that are of typical hydrothermal origin.

The major and trace element composition of clast 86A is significantly different from that of the melt breccias. It shows considerable enrichments in Fe, Mg, Ca, K, P, Sc, V, Co, Ni, Zn, Ga, Rb, Sr, Sb, Cs, Hf, and Th. Sample 86C* shows similar enrichments, but differences in the Cr, Cs, and Ba contents. Sample 86A* in particular shows a rather high concentration of Cr, which probably results from the pyrite which is abundant in the sample. We suggest that the 86 "clasts" formed as hydrothermal fillings of vesicles produced from hot solutions generated by the impact event.

Sample 86A displays a REE pattern similar to that of schistose and quartzitic melt breccias, but has higher absolute abundances. Sample 86C* (REIMOLD and MILLER, 1989) has higher abundances compared to 86A, a similar flat HREE pattern, and is more enriched in LREEs. A characteristic feature of the REE pattern of 86A is a positive Ce anomaly which is often the result of hydrothermal alteration. REIMOLD and MILLER (1989) speculated that these two specimens represented hydrothermally altered inclusions after an ultramafic target rock component, but this assumption is not supported by their chemical composition and the relatively high REE concentrations determined for both of these samples. For example, amphibolite 29* (REIMOLD and MILLER, 1989) has significantly lower REE concentrations. The hypothesis that "clasts" 86A and 86C* are hydrothermal fillings of large vesicles in melt breccias is most consistent with the data.

Schist clast 77* and schist sample 79* (collected at several localities on top of the crater rim as a composite sample of many small chips) differ in composition as a function of the SiO_2, CaO, and volatile contents (Table 2 in REIMOLD and MILLER, 1989). In thin section, both samples closely resemble each other. The trace element chemistry (Table 3 in REIMOLD and MILLER, 1989) for these two samples is also very similar, except for some elements that are mobile under hydrothermal conditions, such as As, Rb, Hf, Cs, Ba, or U, which are enriched in clast 77*. We, therefore, suggest that schist 77* probably contained a secondary carbonate phase. Indeed, calcite pods and crack fillings are frequently observed also in some schistose melt breccias.

Impact-induced hydrothermal events have been documented from several impact craters (see, e.g., PHINNEY et al., 1978; NEWSOM, 1980; NEWSOM et al., 1987; BAIN and KISSIN, 1988; KOMOR et al., 1988; CROSSEY and MCCARVILLE, 1993). The heat induced from the impact, together with severe structural changes that isolate the crater from the surrounding country rock, lead to a hydrothermal system that is restricted to the crater itself. The duration of this post-impact hydrothermal phase is dependent on the size of the crater. While for large craters (>20 km diameter) temperatures may exceed 500°C for many thousand years (NEWSOM, 1980; ALLEN et al., 1982), smaller craters may sustain such temperatures only over a much shorter period of time. However, as shown above, impact-induced hydrothermal alterations may still be recognized even at smaller craters.

SUMMARY AND CONCLUSIONS

The Roter Kamm crater in Namibia has clearly formed by meteorite impact. We found additional evidence for shock metamorphism in further melt breccia samples, including planar deformation features and diaplectic quartz glass in quartz, quartzitic, and, rarely, in granitic clasts. We have studied the petrology, mineralogy, and chemical composition of a number of basement rocks, several melt breccia types, and pseudotachylite-host rock pairs to better define the variety of target rocks, their relation to the various melt breccia types, and any alterations during or after the impact.

The Roter Kamm impact structure exposes a large volume of cataclastic/mylonitic and pseudotachylitic breccias in the basement granite and gneisses, which is unusual for small craters. Field evidence, as well as our chemical and petrological data, suggests that most of these breccias formed by local cataclasis or melting of one specific host rock type, and that only limited evidence for mixing of melts generated from more than one parent rock type is present.

Some of the major observations and conclusions from the present studies are listed below.

1) An objective of this study was a better definition of the pegmatite component in the target and to discriminate it from schist. However, the new pegmatite analyses show some overlap between the compositions of pegmatite and Gariep schist. Some trace elements (e.g., Hf, Ta, U) may be used to identify differences, but, given the coarse-grained nature and the limited outcrop of the pegmatite-derived quartz-feldspar, we consider it futile to perform further mixing calculations to model melt breccia compositions.
2) Three compositional types of melt breccias have been established: (a) the large group of schistose breccias (samples 89C, 87D, 87F, 92A, 52A*, and 52Q*), (b) the quartzitic melt breccias (52B/M*, 87A), and (c) "true" impact melt breccias (41*, 68*) derived by mixing of metasediments and contributions from crystalline basement rocks. Schistose and quartzitic melt breccias dominate the impact melt breccia collection. These melt breccias only rarely contain clasts derived from other country rock types, such as pegmatitic quartz, quartz-feldspar rock, or granite. Schist, quartzite, and sandstone

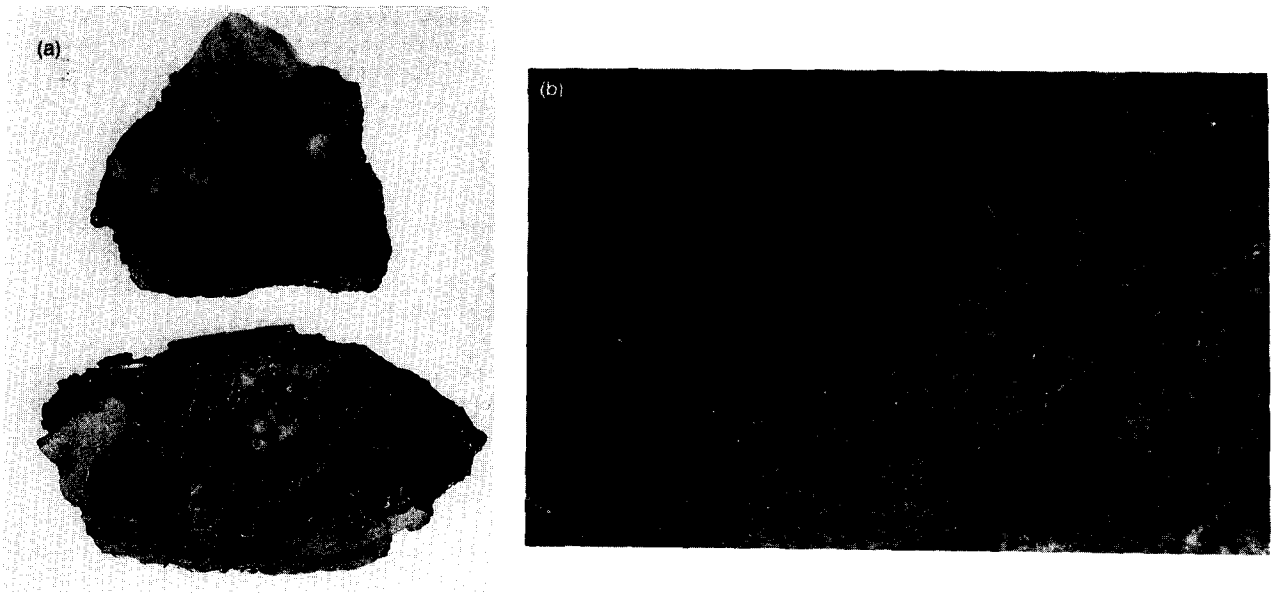

FIG. 10. Clasts in calcrete from outside of the rim of the Roter Kamm crater: (b)–(e): crossed nicols. (a) Two polished slabs of calcrete displaying a variety of clast types; scale bars are 1.75 cm; (b) shocked quartz clast in calcrete sample URK-C1 displaying closely spaced planar deformation features, as well as singular planar fractures (arrows); note that most fluid inclusions cluster along the grain boundary, which was also observed in Witwatersrand quartzite experimentally shocked to shock pressures above ca. 16 GPa (REIMOLD, 1988), and in shocked quartz from impact breccias from the Manson crater (W.U.Reimhold, unpubl. data) (width: 220 μm); (c) two well-rounded partially melted schistose to quartzitic melt breccia clasts (width: 1125 μm); (d) partially fused (and annealed) granitic clast (microcline plus quartz) surrounded by a thin rim of secondary calcite; subplanar fluid inclusion trails in quartz clast at lower left (width: 900 μm); (e) a quartzitic melt breccia clast (upper right corner) and oxidized shale (dark, center left) in calcrete matrix; this photomicrograph also shows marble (m), microcline, quartz, and various types of carbonate clasts; width: 2.2 mm.

or siltstone relics dominate the observed clast populations. Chemical criteria permit minor additions from pegmatite or other basement units in individual cases.

3) The schistose melt breccias as a group show a limited compositional variability for elemental abundances, as well as interelement ratios. Characteristic differences in chemical composition exist between the schistose melt breccias, the quartzitic melt breccias, and the "true" impact melt breccias. Most major element and many trace element concentrations are significantly distinct (by factors of 2–20) between the three breccia types. Such variations exceed any difference in SiO_2 content and are related to different source materials. While distinct in composition from the other melt breccias, the "true" impact melt breccias 41* and 68* are more heterogeneous and show the chemical contribution of their various lithologies, especially granite.
4) None of the target rocks analyzed so far has a composition that is similar to that of the schistose melt breccias, indicating a distinct origin for this breccia group.
5) In contrast to previous interpretations, we now conclude that the schistose melt breccias have formed in situ as monomict breccias, probably involving friction melting. They are not ejected melt breccias, and the shapes, previously thought to be similar to the "flädle" of the Ries crater, can be better explained by erosion followed by surface modification from the abrasive action of sand. The schistose melt breccias have been derived from a confined body of Gariep schist which was part of the local target stratigraphy.
6) The majority of inclusions in calcrete found just outside the crater was derived from sedimentary rocks. In one sample, a shocked quartz crystal with planar deformation features was identified. Quartzitic or schistose melt breccia microclasts are common in the calcrete. Many melt breccia clasts, as well as the schist and siltstone clasts, are well rounded, indicating that the melt clasts are erosional debris fragments from the crater rim.
7) The chemical and mineralogical compositions of pseudotachylitic or mylonitic breccias and their respective host rocks do not indicate that fluids played a major role in reducing melting temperatures during formation of pseudotachylite melt (as previously suggested by, e.g., ERMANOVICS et al., 1972). However, some post-formation alteration seems to have taken place. Differential strain rates and impact-induced movement of basement blocks probably determined whether cataclastic, mylonitic, or pseudotachylitic breccias were formed.
8) Additional support for an impact-induced hydrothermal event was obtained. The presence of large vesicles filled with hydrothermal mineral assemblages in schistose melt breccias (clast samples 86A, 86C*), carbonate fillings of (cooling?) cracks in melt breccias, partial enrichment of melt breccias in mobile trace elements, and the similarity in trace element signatures of melt breccias and hydrothermal vesicle fillings are all consistent with this hy-

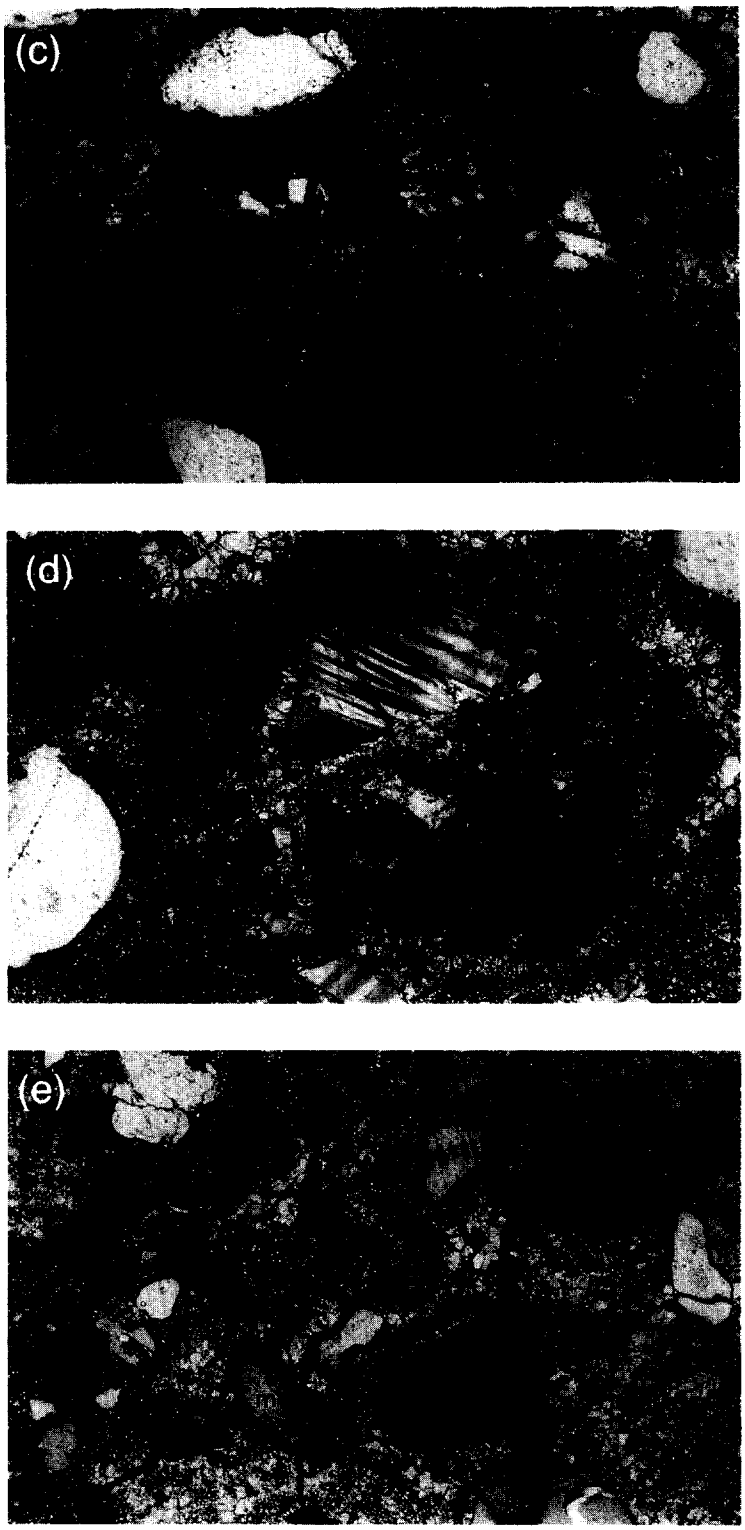

FIG. 10. (Continued)

pothesis. Hydrothermal alteration of basement rocks from the rim is restricted to minor sericitisation and chloritisation mainly observed locally in strongly brecciated or at least jointed rocks, and no carbonate-rich hydrothermal deposits have been recognized in rim specimens. The hydrothermal effects identified in anomalous quartz pebbles and melt breccias is, thus, most likely associated with the immediate post-impact phase.

TABLE 3. MAJOR AND TRACE ELEMENT COMPOSITION OF PSEUDOTACHYLITIC/ MYLONITIC BRECCIA - HOST ROCK PAIRS FROM THE ROTER KAMM CRATER

	ORTHOGNEISS		ORTHOGNEISS		ORTHOGNEISS		MARBLE	
	31B-HR	31B-Myl	38-HR	38-PT	39-HR	39-PT	44A-HR	44A-PT
SiO_2	67.60	63.41	58.71	54.78	66.02	66.90	1.33	8.43
TiO_2	0.35	0.31	0.30	0.26	0.42	0.30	0.02	0.05
Al_2O_3	13.53	14.99	17.11	15.84	15.52	14.23	0.09	0.81
Fe_2O_3	3.82	4.07	6.11	13.62	3.77	4.55	0.29	0.87
MnO	0.06	0.07	0.04	0.01	0.03	0.04	0.02	2.38
MgO	1.83	1.86	1.32	0.90	1.58	1.10	20.83	16.24
CaO	1.33	0.96	0.36	0.25	1.09	0.57	30.45	28.83
Na_2O	3.10	1.42	0.81	0.89	3.08	3.35	0.81	0.65
K_2O	6.90	10.84	13.84	13.40	6.46	8.50	0.01	0.17
P_2O_5	0.20	0.13	0.17	0.13	0.19	0.14	0.02	0.08
L.O.I.	1.75	1.49	1.13	0.65	1.55	0.94	45.51	40.90
Total	100.47	99.55	99.90	100.73	99.71	100.62	99.38	99.41
Sc	9.91	9.50	7.26	3.51	3.98	5.16	0.29	0.59
V	71	n.d.	132	n.d.	147	150	7.4	n.d.
Cr	270	45.1	85	37.3	67	64	8.9	13.6
Co	13.2	13.6	9.92	5.88	11.4	6.44	0.67	11.1
Ni	30	38	<40	<40	39	17	<6	98
Cu	6.6	n.d.	5.8	n.d.	25	25	95	n.d.
Zn	44	47	23	12	66	46	12	118
Ga	6.4	12	12	14	9.3	11	0.2	1.5
As	0.34	4.4	0.57	2.9	0.3	1.57	6.6	5.2
Se	0.6	0.5	2.7	1	0.8	0.3	0.045	0.2
Br	0.8	0.7	0.6	0.7	0.5	<1.5	0.8	1.3
Rb	410	840	1020	930	245	410	2.26	11.1
Sr	205	230	38	<30	256	168	66.4	261
Y	24	n.d.	52	n.d.	17.5	18	1.1	n.d.
Zr	149	116	114	115	310	310	16	26
Nb	5.6	n.d.	12	n.d.	6.5	7.4	0.6	n.d.
Sb	0.17	0.25	0.12	0.13	0.16	0.24	0.025	0.16
Cs	2.34	5.17	2.66	2.38	1.53	1.98	0.04	0.42
Ba	1280	1270	975	780	1470	1270	16	2220
La	62.1	26.7	21.3	10.1	75.4	102	1.25	4.27
Ce	152	62.9	45.4	19.4	161	225	2.26	7.50
Nd	43.3	27.0	19.0	7.8	51.3	68.5	1.1	3.9
Sm	5.15	3.81	3.76	1.77	6.53	8.02	0.27	0.84
Eu	1.20	0.74	0.54	0.30	1.10	1.42	0.058	0.22
Gd	4.0	2.15	2.45	1.4	2.9	4.0	0.3	1.0
Tb	0.64	0.38	0.50	0.29	0.50	0.60	0.054	0.18
Dy	3.8	2.34	4.0	2.65	2.75	3.3	0.3	1.05
Tm	0.28	n.d.	n.d.	n.d.	0.23	n.d.	n.d.	n.d.
Yb	1.85	1.40	4.52	2.60	1.60	1.88	0.17	0.57
Lu	0.26	0.21	0.80	0.51	0.23	0.24	0.023	0.075
Hf	4.86	4.24	3.60	2.93	9.22	8.03	0.10	0.57
Ta	0.49	0.43	2.80	0.94	0.48	0.45	0.017	0.13
W	0.8	0.7	3.7	2.6	0.8	1.1	0.12	1.7
Ir (ppb)	<0.5	<0.7	<0.5	0.7	<0.5	<0.5	<0.5	<0.5
Au (ppb)	10	9.8	2.6	5.8	8	11	38	75
Th	40.6	34.2	31.9	21.5	27.1	39.5	0.29	1.12
U	3.15	2.88	5.52	4.35	2.46	2.1	0.17	0.26
K/U	18159	31203	20785	25537	21770	33555	488	5420
Zr/Hf	30.66	27.36	31.67	39.25	33.62	38.61	160.00	45.61
Hf/Ta	9.92	9.86	1.29	3.12	19.21	17.84	5.88	4.38
La/Th	1.53	0.78	0.67	0.47	2.78	2.58	4.31	3.81
Th/U	12.89	11.88	5.78	4.94	11.02	18.81	1.71	4.31
LaN/YbN	22.68	12.89	3.18	2.63	31.84	36.66	4.97	5.06
Eu/Eu*	0.808	0.790	0.544	0.582	0.772	0.766	0.623	0.734

HR = host rock; PT = pseudotachylite; Myl = mylonite; for other notes see Table 1.

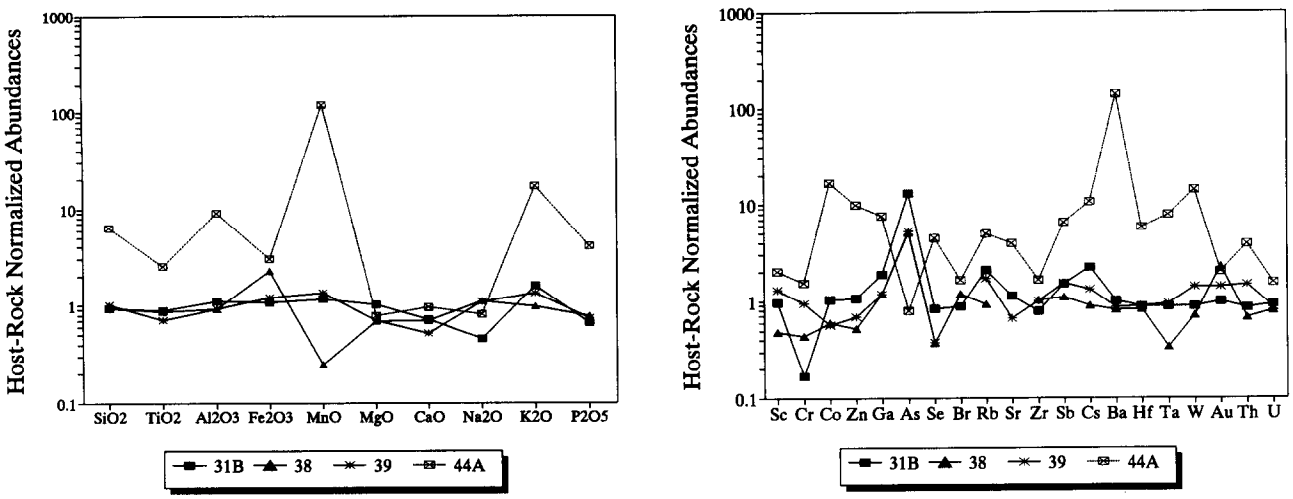

FIG. 11. Host rock-normalized abundances of pseudotachylitic or mylonitic breccias: (a) major elements; (b) trace elements.

9) The chemical and mineralogical observations presented here strengthen the model for the precratering stratigraphy of the target area proposed by REIMOLD and MILLER (1989): dune sand covered a heterogeneous layer of Gariep metasediments, that in turn overlay at least part of the basement lithologies of the Namaqualand Metamorphic Complex, which was also intruded by probably pegmatite-derived quartz-feldspar and associated coarse-grained vein quartz. Not much is known about the thickness of Gariep sediments at the time of impact, but the present height of the crater rim and almost total absence of Gariep deposits on the rim suggest a metasedimentary target layer much less than 100 m thick.

The limited outcrop, the heterogeneity of some target rocks, the scarcity of true (glass-bearing) impact melt breccias, and the extensive sand cover of the crater area indicate that surface studies of the Roter Kamm crater have reached their limits. As this crater is very well preserved and one of the few craters on earth which will allow the determination of important morphometric data (GRIEVE, 1993), we would like to point out the extreme importance of a drilling project at the crater, or alternatively, at least, some detailed geophysical investigations.

Acknowledgments—We gratefully acknowledge Consolidated Diamond Mines (Pty) of Oranjemund for their ongoing interest in our Roter Kamm research and for their permission to carry out field work at the crater structure. Ms. C. Day, Ms. S. Hall, and Mr. V. Govender of the Department of Geology, University of the Witwatersrand, carried out the XRF analyses. We appreciate the support of R. McG. Miller (formerly Director, Geological Survey of Namibia; now NAMCOR, Windhoek) during all aspects of our studies on the Roter Kamm crater. C. K. wants to thank the University of the Witwatersrand, Johannesburg, for a visiting research fellowship during which this paper was finished, and C. Anhaeusser and T. S. McCarthy for the invitation to work at EGRU and the Department of Geology. This study was supported in part by the Austrian FWF, Project No. P8794-GEO (to C.K.). We are grateful to W. v. Engelhardt, B. M. French, R. A. F. Grieve, J. B. Hartung, R. McG. Miller, and H. Palme for helpful comments on various versions of the manuscript.

Editorial handling: H. Palme

REFERENCES

ALLEN C. G., GOODING J. L., and KEIL K. (1982) Hydrothermally altered impact melt rock and breccia: Contributions to the soil of Mars. *J. Geophys. Res.* **87,** 10083–10101.

BAIN J. G. and KISSIN S. A. (1988) A preliminary study of fluid inclusions in shock-metamorphosed sediments at the Haughton impact structure, Devon Island, Canada. *Meteoritics* **23,** 256.

CROSSEY L. J. and MCCARVILLE P. (1993) Post-impact alteration of the Manson impact structure. *Lunar Planet. Sci. XXIV,* 351–352.

DEGENHARDT J. J., BUCHANAN P. C., and REID A. M. (1992) Impactite and pseudotachylite from Roter Kamm crater, Namibia. In *International Conference on Large Meteorite Impacts and Planetary Evolution, Sudbury, Canada,* pp. 20–21. LPI.

DEGENHARDT J. J., BUCHANAN P. C., REID A. M., and MILLER R. McG. (1994) Breccia veins and dykes associated with the Roter Kamm crater, Namibia. In *Large Meteorite Impacts and Planetary Evolution* (ed. B. O. DRESSLER et al.); *GSA Special Paper 293.*

DIETZ R. S. (1965) Roter Kamm, Southwest Africa: Probable meteorite crater. *Meteoritics* **2,** 311–314.

ERMANOVICS I. F., HELMSTAEDT H., and PLANT A. G. (1972) An occurrence of Archean pseudotachylite from South-eastern Manitoba. *Canadian J. Earth Sci.* **9,** 257–265.

FUDALI R. F. (1973) Roter Kamm: Evidence for an impact origin. *Meteoritics* **8,** 245–257.

GRIEVE R. A. F. (1993) Recent studies at the Roter Kamm impact crater. *Meteoritics* **28,** 160.

HARTUNG J. B., KUNK M. J., REIMOLD W. U., MILLER R. M., and GRIEVE R. A. F. (1991) Roter Kamm crater age: 3.5 to 4.0 Ma. *Meteoritics* **26,** 342–343.

HASKIN L. A., HASKIN M. A., FREY F. A., and WILDEMAN T. R. (1968) Relative and absolute terrestrial abundances of the rare earths. In *Origin and Distribution of the Elements* (ed. L. H. AHRENS), pp. 889–911. Pergamon.

KOEBERL C. (1993) Instrumental neutron activation analysis of geochemical and cosmochemical samples: A fast and proven method for small sample analysis. *J. Radioanal. Nucl. Chem.* **168,** 47–60.

KOEBERL C., KLUGER F., and KIESL W. (1987) Rare earth element

determinations at ultratrace abundance levels in geologic materials. *J. Radioanal. Nucl. Chem.* **112,** 481–487.

KOEBERL C., FREDRIKSSON K., GÖTZINGER M., and REIMOLD W. U. (1989) Anomalous quartz from the Roter Kamm impact crater, Namibia: Evidence for post-impact hydrothermal activity? *Geochim. Cosmochim. Acta* **53,** 2113–2118.

KOEBERL C., REIMOLD W. U., BISHOP J., and MILLER R. MCG. (1990a) Roter Kamm impact crater, SWA/Namibia: New geochemical and isotopic studies and further evidence for post-impact hydrothermal activity. *Lunar Planet. Sci. XXI,* 647–648.

KOEBERL C., REIMOLD W. U., GÖTZINGER M., and FREDRIKSSON K. (1990b) Quartz at Roter Kamm crater and post-impact hydrothermal activity: A reply to E. Roedder. *Geochim. Cosmochim. Acta* **54,** 3249–3251.

KOEBERL C., HARTUNG J. B., KUNK M. J., KLEIN J., MATSUDA J. I., NAGAO K., REIMOLD W. U., and STORZER D. (1993) The age of the Roter Kamm impact crater, Namibia: Constraints from ^{40}Ar-^{39}Ar, K-Ar, Rb-Sr, fission-track, and ^{10}Be-^{26}Al studies. *Meteoritics* **28,** 204–212.

KOMOR S. C., VALLEY J. W., and BROWN P. E. (1988) Fluid-inclusion evidence for impact heating at the Siljan Ring, Sweden. *Geology* **16,** 711–715.

MADDOCK R. H. (1986) Partial melting of lithic porphyroclasts in fault-generated pseudotachylytes. *Neues Jahrb. Mineral.* **155,** 1–14.

MADDOCK R. H. (1992) Effects of lithology, cataclasis and melting on the composition of fault-generated pseudotachylytes in Lewisian gneiss, Scotland. *Tectonophysics* **204,** 261–278.

MAGLOUGHLIN J. F. and SPRAY J. F. (1992) Frictional melting processes and products in geological materials: Introduction and discussion. *Tectonophysics* **204,** 197–206.

MILLER R. MCG. and REIMOLD W. U. (1986) Deformation and shock deformation in rocks from the Roter Kamm crater, SWA/Namibia. *Meteoritics* **21,** 456–458.

NEWSOM H. E. (1980) Hydrothermal alteration of impact melt sheets with implications for Mars. *Icarus* **44,** 207–216.

NEWSOM H. E., GRAUP G., SEWARDS T., and KEIL K. (1987) Fluidization and hydrothermal alteration of the suevite deposit at the Ries crater, West Germany, and implications for Mars. *Proc. 17th Lunar Planet. Sci. Conf.; J. Geophys. Res.* **91,** E239–E251.

PHINNEY W. C., SIMONDS C. H., COCHRAN A., and MCGEE P. E. (1978) West Clearwater, Quebec impact structure, Part II: Petrology. *Proc. 9th Lunar Planet. Sci. Conf.,* 2659–2694.

REIMOLD W. U. (1988) Shock experiments with preheated Witwatersrand quartzite and the Vredefort microdeformation controversy. *Lunar Planet. Sci. XIX,* 970–971.

REIMOLD W. U. (1991) The geochemistry of pseudotachylite from the Vredefort Dome, South Africa. *Neues Jahrb. Mineral.* **162,** 151–184.

REIMOLD W. U. and MILLER R. MCG. (1987) Roter Kamm crater, South West Africa/Namibia. In *Excursion Guide: Brukkaros—Roter Kamm Crater Structures, SWA/Namibia* (ed. R. MCG. MILLER and W. U. REIMOLD), pp. 35–87. BPI Geophysics, University of the Witwatersrand.

REIMOLD W. U. and MILLER R. MCG. (1989) The Roter Kamm impact crater, SWA/Namibia. *Proc. 19th Lunar Planet. Sci. Conf.,* 711–732.

REIMOLD W. U., OSKIERSKI W., and HUTH J. (1987) The pseudotachylite from Champagnac in the Rochechouart meteorite crater, France. *Proc. 17th Lunar Planet. Sci. Conf.; J. Geophys. Res.* **92,** E737–E748.

REIMOLD W. U., MILLER R. MCG., GRIEVE R. A. F., and KOEBERL C. (1988) The Roter Kamm impact structure in SWA/Namibia. *Lunar Planet. Sci. XIX,* 972–973.

STOCKEN C. G. (1978) A review of the later Mesozoic and Cenozoic deposits of the Sperrgebiet. *Report for SACS Handbook, Geology Department, Consolidated Diamond Mines, SWA.*

STORZER D., KOEBERL C., and REIMOLD W. U. (1990) Age of the Roter Kamm impact crater, Namibia: A discussion based on fission track and isotopic measurements. *Meteoritics* **25,** 411–412.

WARD J. D. (1987) The Cenozoic succession in Kuiseb Valley, central Namib Desert. *Mem. Geol. Survey of SWA/Namibia* **9.**

WARD J. D., SEELEY M. K., and LANCASTER N. (1983) On the antiquity of the Namib. *South African J. Sci.* **79,** 175–183.

APPENDIX: PETROLOGICAL AND MINERALOGICAL DESCRIPTION OF THE SAMPLES STUDIED IN THE PRESENT WORK. ABBREVIATIONS: QZ = QUARTZ, FSP = FELDSPAR, PLAG = PLAGIOCLASE, DEF = DEFORMATION).

SAMPLE NO	CLASSIFICATION	DESCRIPTION
A. TARGET ROCKS		
URK-123	Pegmatite-derived quartz-feldspar aggregate	Minor plag and microcline set in between up to several cm-large qz crystals; accessory muscovite and Fe-oxides.
URK-75	Pegmatite-derived quartz-feldspar aggregate	Minor amounts of up to >1 cm large plag set in up to 7 mm-large qz crystals. Accessory biotite (partially chloritized), muscovite, perthitic alkali fsp. Plag slightly sericitized. Def: rare irregular fractures in qz and fsp, kinking or shear displacement of plag-twin lamellae. In hand specimen: network of <1 mm wide pseudotachylite or cataclasite veins.
URK-85	Orthogneiss	Coarse-grained (up to 0.8 cm); plag > qz >> alkali feldspar (perthite > orthoclase > microcline); traces of muscovite. Fresh, little sericitisation of fsp. Def: slight - only kinking/shear fracturing in plag.
URK-88	Orthogneiss	Medium-grained; mainly qz, plag, orthoclase, microcline, minor biotite and muscovite; fsp moderately sericitized; def: qz - undulose extinction or def bands; little fracturing, weak plastic def of mica.
URK-89	Orthogneiss	Similar to -88 but biotite more abundant, and fsp more sericitized. Contains several breccia zones (cataclasite, mylonite) <3 mm wide; biotite partially oxidized in breccia, or severely splayed; some annealing along grain boundaries; <1 vol% chlorite, Fe-oxides.

Appendix (Continued)

URK-108	Orthogneiss	Fine to medium-grained, locally granulitic, rock (120° angles) consisting of qz, K-fsp, plag, biotite, some muscovite, and chlorite; biotite and chlorite are concentrated in short, mm-wide layers, possibly remnants of gneiss bands; it appears that the parent gneiss was brecciated which was followed by annealing.
URK-109	Orthogneiss	Strongly annealed granodiorite; consists largely of biotite, qz, relics of K-fsp, and plag (both saussuritized), and secondary epidote; K-fsp and qz are strongly annealed to granular-textured areas; biotite-rich bands could be relics of the former fabric.
URK-110	Orthogneiss	Medium to coarse-grained, well-foliated, slightly folded gneiss; consists of biotite, muscovite, hornblende, and qz; the sample shows a metamorphic overprint that led to partial annealing of qz ± K-fsp.
URK-21 URK-38B	Aplites	Both samples are fine-grained; 21 of mosaic texture, 38B more granoblastic; mineralogy: 21: qz, k-fsp (orthoclase + microcline), plag, minor biotite, muscovite, epidote; 38B: qz, epidote, minor fsp (orthoclase), and partially chloritized biotite. This could imply that 38B was strongly hydrothermally altered to generate about 25 vol% epidote.
URK-83	Qz-fsp-pegmatite (brecciated)	(similar to URK-52I and -26, Miller and Reimold, 1987) Cataclastic and mylonite zones alternate with heavily fractured coherent areas. Locally pseudotachylite-like melt developed. Coherent fragments all qz; in breccia also minor alkali fsp, little plag, traces of biotite clasts. Chlorite occurs interstitially in breccia matrix or in annealed clasts. Intragranular clast def: irregular fracturing, along with incipient annealing.
URK-81A	K-fsp granite (brecciated)	Mylonitic, cataclastic, or pseudotachylitic bands form a network around up to 1 cm large "clasts" of orthogneiss or coherent gneiss. Def: undulose extinction and irregular fracturing in qz and fsp, strong cleavage in fsp, biotite is strongly sheared. Some devitrified glass, some brownish aphanitic areas (after biotite) with schlieren. Noticeable alteration: relics of mafic minerals in "clasts" and breccia zones are strongly chloritized, some carbonate patches along joints, and a greenish clay mineral after melt. Mineralogy of (medium-grained) parent rock: perthitic alkali fsp + microcline > qz > plag > biotite (+ alteration products) (Fig. 5c).
URK-81B	Orthogneiss (brecciated)	Parent rock: 20 vol% biotite, qz > alkali fsp > plag; significant fsp alteration, biotite-gneiss oxidation of biotite - probably related to brecciation event. Def.: biotite kinked and splayed, fsp + qz strongly fractured. Host rock annealing far less than in mylonitic samples. Clasts are mainly qz or granite-gneiss. Areas with aphanitic matrix next to very fine-grained granoblastic melt rock or cataclasite. Clasts frequently annealed, roundish, some chlorite.
URK-73A	Calcareous sandstone	Fine-grained (mostly <250 μm) angular to subrounded qz forms up to 4 mm aggregates or is set individually into finer-grained carbonate matrix (Calcite >> dolomite). No evidence for post-formational def (Fig. 5a).
B. Melt Breccias		
URK-87A	Quartzitic melt breccia	Highly siliceous melt rock, completely annealed, with few K-fsp, muscovite, or qz-fsp-pegmatite clasts (up to 5 cm in size). Some roundish vesicles contain very fine-grained qz-carbonate-chlorite mineralization. Clasts are generally undeformed; only one is partially fused/annealed. One partially melted (vesicles)/oxidized biotite clast, similar to stage 4 shock deformation (Stöffler, 1971) (Fig. 5b).

Appendix (Continued)

URK-87C	"Schistose" melt breccia	Cf. Miller and Reimold (1987) and Reimold and Miller (1989) for terminology. Patches of very fine-grained devitrified or crystalline SiO_2 -rich melt alternate with partially melted or oxidized schist on a mm to cm-scale. The sample contains several quartzite clasts (probably resulting from Gariep schist interbanded with quartzitic layers), dark oxides (after siltstone?), and carbon. Many clasts are partially fused. No shock def detected.
URK-87D	"Schistose" melt breccia	Similar to 87C, but siltstone clasts more abundant. Up to 1 cm long ovoid vesicles filled with conchoidal/radiating qz - in the center voids or dark brownish glass. The clasts show no shock effects.
URK-87F	"Schistose" melt breccia	Similar to 87C, but higher quartzite to siltstone/schist ratio.
URK-92A	"Schistose" melt breccia	Many qz and qz-muscovite clasts, often partially melted. One clast with strong mosaicism and patchy annealing (Fig. 6b), and planar features in some unannealed domains. Several other qz clasts with single set of planar deformation features.
URK-86A	Clast in melt breccia	Belongs to a group of three samples (86A-C) occurring as 6-10 cm large clasts in "schistose" melt breccias. They consist of a central core surrounded by a dark-green, up to 1 cm wide rim. The core is composed of a phlogopite-like mica with variable amounts of pyrite, qz, possibly clinohumite, apatite and zircon as trace minerals, and several vol% chlorite. Some interstices contain plag. The rim is primarily composed of chlorite with variable amounts of light mica and pyrite which mostly forms well-developed laths or irregular roundish aggregates (euhedral cubic shapes were observed as well) (Fig. 6d,e).
C. Pseudotachylitic/Mylonitic Breccia - Host Rock Pairs		
URK-31B	Orthogneiss/ mylonite	Microcline-granitic gneiss; mainly microcline + qz, minor biotite and plag; strong strainbanding and irregular fracturing. In wedge-shaped zones mylonitized (perhaps local pseudotachylite development). Some clasts annealed, matrix partially chloritized.
URK-38	Orthogneiss/ pseudotachylite	Weakly foliated granite-gneiss consisting of plag, orthoclase + microcline, qz. In melt zone growth of euhedral magnetite (± ilmenite). Little biotite in parent gneiss.
URK-39	Orthogneiss/ pseudotachylite	Similar to URK-38, but less melt. Mostly microcline + qz, some plag. Strong sericitisation, annealing (granophyric patches, i.e., partial melting), chloritized biotite.
URK-44	Marble/ pseudotachylite	Very fine-grained marble (calcite + dolomite) with minor qz (<2 vol%) and some Fe-oxides. The breccia consists of dark-brown matrix enriched in up to 100 µm-sized Fe- and Mn-oxide crystals, also some muscovite and larger quartzite aggregates.